



HAL
open science

Kinetic Study of the Gas-Phase Reaction between Atomic Carbon and Acetone: Low-Temperature Rate Constants and Hydrogen Atom Product Yields

Kevin Hickson, Jean-Christophe Loison, Valentine Wakelam

► **To cite this version:**

Kevin Hickson, Jean-Christophe Loison, Valentine Wakelam. Kinetic Study of the Gas-Phase Reaction between Atomic Carbon and Acetone: Low-Temperature Rate Constants and Hydrogen Atom Product Yields. ACS Earth and Space Chemistry, 2023, 7 (10), pp.2091-2104. 10.1021/acsearthspacechem.3c00193 . hal-04235188

HAL Id: hal-04235188

<https://hal.science/hal-04235188v1>

Submitted on 11 Oct 2024

HAL is a multi-disciplinary open access archive for the deposit and dissemination of scientific research documents, whether they are published or not. The documents may come from teaching and research institutions in France or abroad, or from public or private research centers.

L'archive ouverte pluridisciplinaire **HAL**, est destinée au dépôt et à la diffusion de documents scientifiques de niveau recherche, publiés ou non, émanant des établissements d'enseignement et de recherche français ou étrangers, des laboratoires publics ou privés.

Kinetic Study of the Gas-Phase Reaction between Atomic Carbon and Acetone. Low Temperature Rate Constants and Hydrogen Atom Product Yields

Kevin M. Hickson,^{1,*} Jean-Christophe Loison,¹ and Valentine Wakelam²

¹Institut des Sciences Moléculaires ISM, CNRS UMR 5255, Univ. Bordeaux, 351 Cours de la Libération, F-33400, Talence, France

²Laboratoire d'astrophysique de Bordeaux, CNRS, Univ. Bordeaux, B18N, allée Geoffroy Saint-Hilaire, F-33615 Pessac, France

Abstract

The reactions of ground state atomic carbon, C(³P), are likely to be important in astrochemistry due to the high abundance levels of these atoms in the dense interstellar medium. Here we present a study of the gas-phase reaction between C(³P) and acetone, CH₃COCH₃. Experimentally, rate constants were measured for this process over the 50-296 K range using a continuous-flow supersonic reactor, while secondary measurements of H(²S) atom formation were also performed over the 75-296 K range to elucidate the preferred product channels. C(³P) atoms were generated by In-situ pulsed photolysis of carbon tetrabromide, while both C(³P) and H(²S) atoms were detected by pulsed laser induced fluorescence. Theoretically, quantum chemical calculations were performed to obtain the various complexes, adducts and transition states involved in the C(³P) + CH₃COCH₃ reaction over the ³A'' potential energy surface, allowing us to better understand the reaction pathways and help to interpret the experimental results. The derived rate constants are large, (2-3) × 10⁻¹⁰ cm³ s⁻¹, displaying only weak temperature variations; a result that is consistent with the barrierless nature of the reaction. As this reaction is not present in current astrochemical networks, its influence on simulated interstellar acetone abundances is tested using a gas-grain dense interstellar cloud model. For interstellar modelling purposes, the use of a temperature independent value for the rate constant, $k_{C+CH_3COCH_3} = 2.2 \times 10^{-10} \text{ cm}^3 \text{ s}^{-1}$, is recommended. The C(³P) + CH₃COCH₃ reaction decreases gas-phase CH₃COCH₃ abundances by as much as two orders of magnitude at early and intermediate cloud ages.

1 Introduction

Carbon bearing compounds are ubiquitous throughout the Universe, with carbon being present as the fourth most abundant element following H, He and O. In interstellar space, elemental carbon is considered to be mostly present as C^+ in diffuse clouds (here elements with an ionization potential < 13.6 eV are generally considered to be fully ionized), before transforming into neutral atomic carbon $C(^3P)$ and initially, simple molecular species (CO, CH, CH_2 , CH_3) in denser regions of interstellar space. Observations of neutral atomic carbon towards dense molecular clouds such as TMC-1,¹ OMC-1^{2,3} and Barnard 5⁴ through the $C(^3P_1-^3P_0)$ and $C(^3P_2-^3P_1)$ fine structure transitions in the submillimeter-wave range at 492.162 GHz and 809.345 GHz clearly indicate that neutral atomic carbon and CO coexist deep inside these clouds. Indeed, recent models⁵ predict that neutral atomic carbon abundances could be as high as 10^{-4} (relative to H_2) during the early stages of cloud evolution. In this respect, it is important to investigate the reactivity of $C(^3P)$ with a wide range of interstellar molecules to evaluate their potential importance to the overall chemistry of these regions. Although there are numerous studies of the kinetics⁶⁻⁹ and dynamics^{7,9-13} of $C(^3P)$ reactions with a wide range of unsaturated hydrocarbons, there are relatively few studies of its reactions with organic molecules containing other types of functional groups such as those found in complex organic molecules (COMs). Over the last few years, we have begun to address this issue by examining the reactivity of $C(^3P)$ with important COMs such as CH_3OH ¹⁴ and CH_3CN ¹⁵ and other molecules that are thought to be formed primarily on interstellar ices such as N_2O .⁵

At the present time, the chemical processes leading to the formation of many of the observed interstellar COMs are not well constrained in a general sense. Among them, acetone, CH_3COCH_3 , was first detected in the dense molecular cloud Sgr B2 (OH) by Combes et al.¹⁶ in 1987 with a derived column density of $5 \times 10^{13} \text{ cm}^{-2}$ corresponding to a relative

abundance (with respect to H₂) of 5×10^{-11} . Its detection was subsequently confirmed by Snyder et al.¹⁷ who observed several transitions towards Sgr B2 (OH), Sgr B2 (M) and Sgr B2 (N), while confirming that acetone emission arose predominantly from the hot molecular core Sgr B2 (N-LMH). They derived much higher relative abundances, $(4-30) \times 10^{-10}$, compared to those obtained by Combes et al.¹⁶ Very recently, acetone has been detected at the cyanopolyne peak position of the prototypical cold dark cloud TMC-1, through the QUIJOTE survey observations with an abundance of 1.4×10^{-11} .¹⁸ Acetone has also been observed in several other interstellar environments including the high mass star forming regions GAL 31.41+0.31, GAL 034.3+00.2, and GAL 10.47+00.03¹⁹ with column densities in the range $(0.1-1.3) \times 10^{15} \text{ cm}^{-2}$ and towards the low-mass protostar IRAS 16293-2422²⁰ with a column density of $1.7 \times 10^{16} \text{ cm}^{-2}$.

In terms of its production in the gas-phase ISM, acetone can be formed from acetaldehyde (CH₃CHO) by the radiative association reaction $\text{CH}_3^+ + \text{CH}_3\text{CHO} \rightarrow (\text{CH}_3)_2\text{CHO}^+ + h\nu$ followed by dissociative recombination $(\text{CH}_3)_2\text{CHO}^+ + e^- \rightarrow \text{CH}_3\text{COCH}_3 + \text{H}$, but certain models²¹ have shown that this process largely underestimates observed abundances. The neutral-neutral reaction between atomic oxygen and C₃H₇ is also considered to be a minor source.²² Acetone is lost through ion-molecule reactions with several cations such as H₃⁺, HCO⁺, He⁺ and H₃O⁺.²² Although it does not react with the other abundant interstellar atomic radicals N(⁴S) and O(³P) at low temperature in the gas-phase, acetone has been shown to react with small hydrogen bearing radicals such as CH²³ and OH.^{24,25} Although the OH + acetone reaction has not been conclusively demonstrated to lead to reaction products through direct measurements (as opposed to complex stabilization through collisions with the carrier gas), this process is nonetheless included in current astrochemical databases, while

rate constants for the CH + acetone reaction have never been measured so this reaction is not currently included.²²

Instead, modeling studies have highlighted the probable influence of the formation of complex organic molecules (COMs) in general through neutral-neutral reactions on the surface of ice-covered interstellar dust grains. It has been suggested that the reaction of CH₃ with CH₃CO²⁶ followed by chemical desorption of a fraction of the surface formed products could be an important source of gas-phase acetone. Nevertheless, as the observed gas-phase acetone abundances are not well reproduced by astrochemical models, this seems to indicate that important gas-phase or surface reactions leading to acetone formation are poorly constrained or missing entirely from current networks.

In order to improve the current knowledge of acetone chemistry in the interstellar medium, we have undertaken an experimental investigation of the gas-phase C(³P) + acetone reaction over the 50-296 K temperature range using a continuous supersonic flow apparatus, coupled with pulsed laser photolysis and pulsed laser induced fluorescence for C(³P) atom formation and detection respectively. In addition to the kinetic measurements, we have also performed measurements of the product channels leading to atomic hydrogen formation at room temperature and below. In conjunction with new electronic structure calculations of the various complexes, intermediates and transition states over the triplet potential energy surface (PES), this work has allowed us to identify the major product channels for interstellar modeling studies. Finally, we have tested the effect of the C(³P) + acetone reaction on a dense cloud model while updating the chemistry leading to acetone formation and loss in both the gas-phase and on interstellar ices.

The experimental and theoretical methods employed are described in sections 2 and 3 respectively, while the results of this work are presented in section 4. The astrochemical

simulations and the implications of this study for interstellar acetone and related species are described in section 5, followed by our conclusions in section 6.

2 Experimental Methods

All the experiments described here were performed using a supersonic flow reactor, also known by the French acronym CRESU (Cinétique de Réaction en Écoulement Supersonique Uniforme or Reaction Kinetics in a Uniform Supersonic Flow). This apparatus, which has been described in detail in earlier work,^{27,28} employs axisymmetric Laval nozzles to generate low temperature flows with uniform density, temperature and velocity characteristics over a known distance from the nozzle, allowing the kinetics of fast gas-phase reactions to be investigated (with rate constants $> 10^{-12} \text{ cm}^3 \text{ s}^{-1}$). Since these early studies, numerous modifications have been made, notably allowing the detection of atomic species in ground ($\text{C}(^3\text{P})$,^{29, 30} $\text{H}(^2\text{S})$ ^{31,32}) and excited ($\text{O}(^1\text{D})$,^{33,34} $\text{N}(^2\text{D})$ ^{35,36}) electronic states through their transitions in the vacuum ultraviolet wavelength range. Measurements were performed at five different temperatures during the present work (296 K, 177 K, 127 K, 75 K, 50 K) with N_2 or Ar as the carrier gases. Three different Laval nozzles were used to access temperatures below 296 K (one nozzle was employed with both N_2 and Ar, allowing flow temperatures of 177 K and 127 K to be generated respectively). The nozzle flow characteristics are summarized in Table 2 of Hickson et al.³¹ For each temperature, the distance between the Laval nozzle exit and the observation axis was set to the maximum value for which the flow conditions could still be considered optimal, providing us with the maximum possible time to record kinetic profiles. These characteristic distances were derived in earlier experiments measuring the supersonic flow impact pressure as a function of distance from the nozzle using a Pitot tube.

The nozzle was removed to perform room temperature experiments, with a reduced flow velocity to eliminate pressure gradients within the reactor.

Acetone was introduced into the flow via a temperature- and pressure-controlled bubbler system upstream of the Laval nozzle. Here, a small fraction of the carrier gas flow (< 25 sccm) was diverted into a bubbler containing acetone maintained at room temperature and a pressure around 400 Torr. The acetone laden carrier gas was then flowed into a cold trap maintained at 17 °C, allowing the gas-phase acetone concentration at the trap exit to be calculated precisely using its saturated vapour pressure at this temperature.³⁷ The output of the cold trap was connected to the Laval nozzle reservoir through a tube heated to 80 °C to prevent condensation before further dilution by the remaining carrier gas flows. In this case, the use of the heated tube was simply a precautionary measure as no condensation losses were ever observed during experiments with and without heating.

In common with our earlier studies of C(³P) reactivity at low temperature, carbon tetrabromide (CBr₄) was used as the precursor molecule in the present work. These molecules were entrained in the flow by passing a small fraction (40 – 70 sccm) of the total flow over solid CBr₄ maintained at a known fixed pressure and room temperature in a separate vacuum flask. CBr₄ concentrations in the supersonic flow were estimated to be lower than 2.6×10^{13} cm⁻³ based on its saturated vapour pressure. C(³P) atoms were produced directly in the cold supersonic flow by the 266 nm pulsed laser photolysis of CBr₄ at 10 Hz. This beam (with pulse energies of 30-35 mJ for a 5 mm beam diameter) was steered in through the back of the reactor via a fused silica window oriented at the Brewster angle to reduce window fluorescence, and was coaligned along the supersonic flow, exiting by the nozzle throat and a second Brewster angled window positioned at the back of the reservoir. In this way, a column of C(³P) atoms was produced along the entire length of the supersonic flow, with the nascent

C(³P) concentration being identical at any axial position, due to the weak attenuation of the UV beam by CBr₄ ($\sigma_{\text{CBr}_4}(266 \text{ nm}) = 1 \times 10^{-18} \text{ cm}^2$). It should be noted that under our experimental conditions, CBr₄ photolysis at 266 nm also produces some excited state C(¹D) atoms at the level of 10-15 %.¹⁴ The possible interferences brought about by the presence of these atoms are discussed in section 4.

C(³P) atoms were detected directly during the present kinetic experiments by pulsed laser induced fluorescence in the vacuum ultraviolet wavelength range through the $2s^2 2p^2 \text{ } ^3\text{P}_2 \rightarrow 2s^2 2p5d \text{ } ^3\text{D}_3^\circ$ transition at 115.803 nm. Tunable radiation around this wavelength was produced by the second harmonic generation of the output from a narrowband dye laser at 695 nm, itself pumped by the second harmonic output (532 nm) of a 10 Hz pulsed Nd:YAG laser. The residual 695 nm radiation after doubling was eliminated from the UV beam at 347 nm using two dichroic mirrors coated for maximal reflection at 355 nm. The pulse energy was typically 8-9 mJ for a 5 mm beam diameter. Part of the discarded visible radiation was fed into the input coupler of a wavelength meter allowing us to track the probe laser wavelength variations in real time. The 347 nm beam itself was steered using right angled prisms and was focused into a gas cell attached to the reactor at the level of the observation axis (and at right angles to the supersonic flow) via a 75 cm arm. The cell contained 50 Torr of xenon with 160 Torr of argon for optimal phase matching, allowing us to generate the required tunable VUV radiation around 115.8 nm by frequency tripling. For the H-atom product detection experiments, tunable radiation around the Lyman- α transition at 121.567 nm was generated in a similar manner, with the dye laser operating at 729 nm and a mixture of 210 Torr of krypton and 540 Torr of argon in the tripling cell.

As the VUV beam was divergent as it left the cell, a MgF₂ lens was used instead of a plane window at the cell exit to recollimate the beam before entering the reactor where it

was allowed to interact with the supersonic flow. Due to the difference in refractive index of MgF_2 at VUV and UV wavelengths, the UV beam diverged along the input arm, allowing a large fraction of this radiation to be blocked by a series of circular diaphragms positioned at various distances between the cell and the reactor, although a small fraction of the UV beam did still interact with the supersonic flow. As the arm was open to the reactor, containing species such as CBr_4 and CH_3COCH_3 which absorb strongly in the VUV range, this zone was flushed continuously by a flow of Ar or N_2 during the experiments. To check that the residual UV beam entering the reactor did not affect the measurements, several test experiments were performed. First, at the start of the initial experiments measuring rate constants and H-atom branching ratios, the cell was evacuated to ensure that no spurious signals were observed in the absence of VUV light. Similarly, preliminary experiments were also performed in the absence of the photolysis laser (with and without gas in the tripling cell) to check for the formation of $\text{C}(^3\text{P})$ and/or $\text{H}(^2\text{S})$ by either the VUV beam or the residual UV beam. No signal from $\text{C}(^3\text{P})$ was ever observed, but a small H-atom fluorescence signal was observed when CH_3COCH_3 was present in the flow and gas was present in the tripling cell, due to CH_3COCH_3 photolysis by the VUV probe beam at 121.567 nm. In this case, this signal did not vary as a function of time (as the probe laser energy was fixed). Additionally, a larger H-atom fluorescence signal was observed with CH_3COCH_3 in the flow with both the photolysis and VUV probe lasers on, arising from CH_3COCH_3 photolysis at 266 nm. An explanation of how we disentangled the contribution of the H-atom photolysis signal from the H-atom reactive signal is provided in section 4.3. The fluorescence emission from C- or H- atoms within the flow was detected at right angles to both the supersonic flow and the VUV beam. The detection system consisted of a solar blind photomultiplier tube (PMT), isolated from the reactor by a LiF window, while a series of circular diaphragms were placed along the detection axis to reduce

the detection of scattered light. Within the isolated region, which was evacuated by an oil-free vacuum pump to prevent atmospheric absorption losses, a LiF lens focused the VUV emission onto the PMT photocathode. The output signal from the PMT was fed into a gated boxcar integrator, with the boxcar system, oscilloscope (for signal visualization and gate positioning) and both lasers being synchronized by a digital pulse generator. C(³P) and H(²S) fluorescence signals were recorded as a function of time, with each time point consisting of 30 individual laser shots. For each temporal scan, at least 100 time points were typically recorded, with at least 15 of them at negative time delays (that is, with the probe laser firing prior to the photolysis laser). These points allowed us to establish the baseline level, which consisted of any scattered light signals and, in the case of the H-atom detection experiments, the small contribution of H-atom fluorescence from CH₃COCH₃ photolysis by the VUV probe laser as described above.

The carrier gas flows used in the present experiments Ar (Messer 99.999 %) and N₂ (Messer 99.999 %) were regulated by calibrated mass-flow controllers. All gases including the rare gases used in the tripling cell, Xe (Linde 99.999 %) and Kr (Linde 99.999 %), were flowed from their cylinders directly without purification.

3 Electronic Structure Calculations

As reaction is expected to occur over the ground triplet state of the C + CH₃COCH₃ system, this PES was investigated at different levels of theory. In the first instance, the geometries and energies of the reagents, intermediates, transition states (TSs) and possible products were calculated using density functional theory (DFT) employing the M06-2X functional³⁸ coupled with the aug-cc-pVTZ (AVTZ) basis set. This functional has been shown to have good accuracy for the prediction of main-group thermochemistry, kinetics, barrier heights and non-

covalent interactions.³⁹ At the same time, harmonic frequencies were also calculated for these structures at the same level in order to verify the nature of the stationary point (a single imaginary frequency for a TS, no imaginary frequencies for a minimum or product/reagent species). In addition, intrinsic reaction coordinate calculations were performed to confirm that each TS lies on the minimum energy path between 2 assumed minima. For certain critical structures, such as those species that were predicted to lie close in energy to the reagent asymptote at the M06-2X/AVTZ level, we ran more accurate energy calculations based on the geometries obtained at the M06-2X/AVTZ level using the domain based local pair-natural orbital singles and doubles coupled cluster theory with an improved perturbative triples correction algorithm (DLPNO-CCSD(T)).⁴⁰ This approach was favoured over standard CCSD(T) calculations due to the large gain in computational time which was further improved by the application of the RIJCOSX approximation.⁴¹ In common with the DFT calculations, the DLPNO-CCSD(T) method was associated with the AVTZ basis set for these calculations. All calculations were performed using ORCA,^{42, 43} while the vibrational frequency analysis and structure visualization were performed using Avogadro.⁴⁴

4 Results

4.1 Potential Energy Surface

A schematic representation of the $^3A''$ surface involved in the $C + CH_3COCH_3$ reaction is shown in Figure 1.

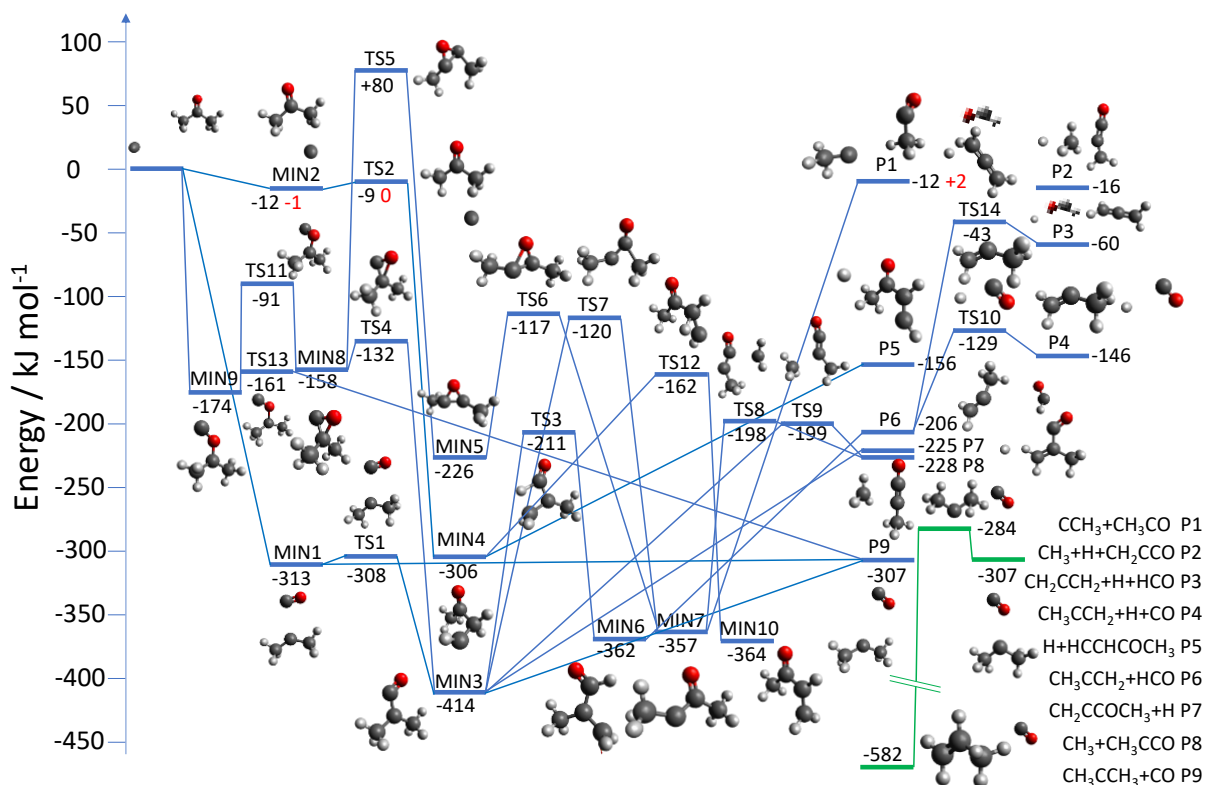


Figure 1 Schematic diagram of the triplet potential energy surface for the $C(^3P) + CH_3COCH_3$ reaction with energies obtained at the M06-2X/AVTZ level. Certain structures close in energy to the reagent asymptote at this level were calculated with the more accurate DLPNO-CCSD(T)/AVTZ method (energy values in red). Relevant parts of the singlet potential energy surface for the isomerization of 1H_3CCCH_3 to 1CH_3CHCH_2 (propene) are also shown. All energies were corrected for zero-point energy differences.

Energies are displayed at the M06-2X/AVTZ level, with certain critical energies in red displayed at the DLPNO-CCSD(T)/AVTZ level. All energies are corrected for ZPE differences (ZPEs were obtained at the M06-2X/AVTZ level) derived from a vibrational frequency analysis. The green line represents the singlet surface connecting species 1CH_3CCH_3 with 1CH_3CHCH_2 . Ten different minima were identified during this work, with nine different product sets connected by fourteen TSs. There are almost certainly several other minima, transition states

and product channels that are also energetically accessible, although we believe that we have identified the most important ones to explain the results of our investigation. According to our calculations, ground-state atomic carbon can attack CH_3COCH_3 at two different positions in a similar manner to the entrance channels predicted by Joo et al.⁴⁵ for the related $\text{C} + \text{H}_2\text{CO}$ reaction.

As a first step, atomic carbon can approach the oxygen atom of the carbonyl group. Here, the C-atom either inserts into the C-O bond of CH_3COCH_3 leading to the formation of intermediate species MIN1, 313 kJ/mol below the reagents at the M06-2X/AVTZ level or it adds to the O-atom to form MIN9, -174 kJ/mol below the reagents at the M06-2X/AVTZ level with both approaches being barrierless. MIN1, a weakly bound complex between CH_3CCH_3 and CO can either rearrange to MIN3 after overcoming a very low barrier (TS1) of only 5 kJ/mol with respect to MIN1 or dissociate directly to the separated products, ${}^3\text{CH}_3\text{CCH}_3 + {}^1\text{CO}$ (P9), 307 kJ/mol below the reagents. MIN9 can dissociate to products P9 after passing over a low TS (TS13) only 13 kJ/mol above MIN9, or it can isomerize to the cyclic intermediate MIN8 through a TS 91 kJ/mol below the reagent level (TS11). Once MIN8 is formed, C-O bond breaking can occur (the atoms of the original C=O bond of acetone are those involved here in TS4) to form MIN3. Additional evolution of MIN8 towards another cyclic intermediate MIN5 can only occur over a high barrier, TS5, 238 kJ/mol above MIN8 and 80 kJ/mol above the reagent energy level so this pathway will not occur under the low temperature conditions of the present experiments.

MIN3, potentially formed by both channels $\text{MIN1} \rightarrow \text{TS1} \rightarrow \text{MIN3}$ and $\text{MIN9} \rightarrow \text{TS11} \rightarrow \text{MIN8} \rightarrow \text{TS4} \rightarrow \text{MIN3}$, can isomerize through several energetically accessible pathways to form MIN6 via H-atom transfer over TS3 (213 kJ/mol above MIN3) and MIN7 via CH_3 transfer over TS7 (294 kJ/mol above MIN3). MIN3 is also predicted to form bimolecular

products through three different pathways. MIN3 can dissociate directly via C-H bond fission to $\text{CH}_2\text{CCOCH}_3 + \text{H}$ products (P7), 225 kJ/mol below the reagents or it can dissociate via C-C bond fission to $\text{CH}_3 + \text{CH}_3\text{CCO}$ products (P8), 228 kJ/mol below the reagents after passage over an exit TS (TS9) 29 kJ/mol above P8. The C-C bond that breaks here was one of those already present in the CH_3COCH_3 molecule. Alternatively, MIN3 can also dissociate directly to products P9 by breaking the newly formed C-C bond.

Once formed, MIN6 can dissociate via C-C bond breaking directly to products $\text{CH}_3\text{CCH}_2 + \text{HCO}$ (P6), 206 kJ/mol below the reagents. MIN7 can dissociate to products P8 after fission of the C-C bond between the methyl group and the C-atom of the carbonyl group. This pathway involves an exit TS (TS8) 30 kJ/mol above the P8 asymptote. Alternatively, after fission of the C-C bond on the other side of the carbonyl group, MIN7 can dissociate directly to products $\text{CCH}_3 + \text{CH}_3\text{CO}$ (P1), slightly below the reagents at the M06-2X/AVTZ level (-12 kJ/mol). The energy of these products at the DLPNO-CCSD(T)/AVTZ level is +2 kJ/mol (corrected for ZPE), so that this channel may not play any part in the present low temperature experiments. As a third possible pathway, MIN7 can isomerize to MIN5 over TS6, located 240 kJ/mol above MIN7.

For the $\text{C} + \text{CH}_3\text{COCH}_3$ reaction, an alternative pathway exists that is not available in the $\text{C} + \text{H}_2\text{CO}$ reaction.⁴⁵ Here, atomic carbon can insert into a C-H bond of one of the methyl groups of CH_3COCH_3 to form a weakly bound (-12 kJ/mol at the M06-2X/AVTZ level) van der Waals type complex MIN2. MIN2 can isomerize to MIN4 over TS2, 9kJ/mol below the reagents at the M06-2X/AVTZ level. The calculated energies at the DLPNO-CCSD(T)/AVTZ level are -1 and +0.5 kJ/mol for MIN2 and TS2 respectively, when zero-point-energy corrections (evaluated at the M06-2X/AVTZ level) are taken into account. Given the expected precision of the calculated energies which have been estimated to be within less than 3 kJ/mol of the

canonical CCSD(T) results for open-shell systems,⁴⁶ it is entirely possible that this represents a non-negligible reaction pathway, particularly at low temperature. After the MIN4 intermediate is formed, this species can isomerize to MIN10 over TS12, 144 kJ/mol above MIN4 or evolve to products H + HCCHCOCH₃ (P5) (150 kJ/mol above MIN4) via C-H bond dissociation without a barrier.

Intersystem crossing

Interestingly, one of the major products predicted to be formed, ³CH₃CCH₃, could also evolve further in this scenario. This species could undergo intersystem crossing to the singlet state, as ¹CH₃CCH₃ (shown in green in Figure 1) is calculated to be at the same energy as the triplet state species at the M06-2X/AVTZ level. Moreover, the geometries of these species are quite similar as the C-C and C-H bond lengths are very close with the only major difference being the C-C-C angles which are 132° and 112° for the triplet and singlet forms respectively, accompanied by different rotational positions of the methyl group hydrogens (see Figure 2).

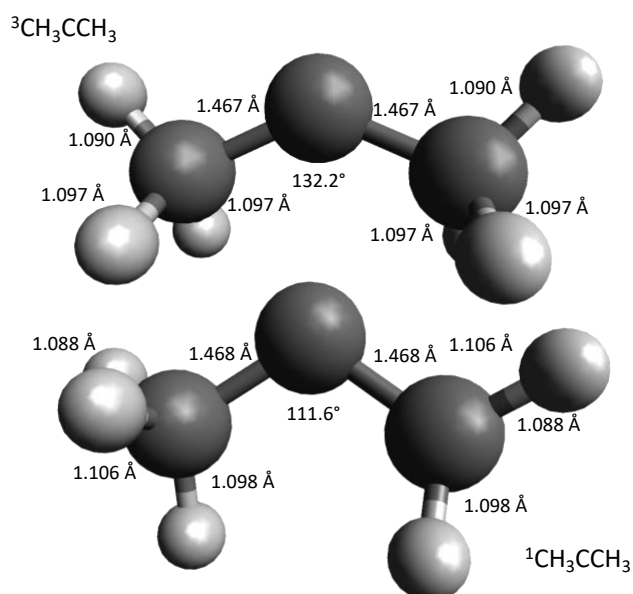


Figure 2 Calculated geometries of the CH₃CCH₃ molecule at the M06-2X/AVTZ level in its singlet and triplet state electronic configurations.

In order to check whether intersystem crossing might occur in this case, we ran a minimum energy crossing point (MECP) optimization to determine its energy. The MECP is found to occur only +15 kJ/mol (corrected for ZPE) above the $^3\text{CH}_3\text{CCH}_3$ minimum at the M06-2X/AVTZ level. Once $^1\text{CH}_3\text{CCH}_3$ is formed it can isomerize to propene, C_3H_6 , 275 kJ/mol below $^1\text{CH}_3\text{CCH}_3$ after overcoming a low TS of +23 kJ/mol relative to $^1\text{CH}_3\text{CCH}_3$. Considering the energetically favourable pathways towards C_3H_6 formation and the possible large branching fraction for the formation of P9 products, if the $\text{C} + \text{CH}_3\text{COCH}_3$ reaction is rapid at low temperature, it could represent a gas-phase source of propene in the dense ISM.

4.2 Rate constants

Acetone was present in the flow with a large excess concentration with respect to $\text{C}(^3\text{P})$ during these experiments. Consequently, its concentration was considered to be constant during the individual runs, so it was possible to analyze the kinetics of the $\text{C}(^3\text{P}) + \text{acetone}$ reaction using a pseudo-first-order treatment. As CBr_4 photolysis also produces some $\text{C}(^1\text{D})$ in the flow, it is important to consider whether these atoms might interfere with the rate constant measurements by relaxing back to the ground state or by reacting on the timescale of the experiment. As $\text{C}(^1\text{D})$ is not detected during these experiments while $\text{C}(^3\text{P})$ atoms are detected directly, the expected rapid reaction of $\text{C}(^1\text{D})$ with acetone will not affect the kinetic measurements performed here. Furthermore, as $\text{C}(^1\text{D})$ quenching by Ar is slow,⁴⁷ these atoms should not interfere with the rate constant measurements when Ar is used as the carrier gas. When N_2 is used as the carrier gas, such as during the experiments conducted at 177 K, $\text{C}(^1\text{D})$ quenching will occur rapidly with a half-life time, $t_{1/2}$, $< 1 \mu\text{s}$ for an N_2 flow density of $9.4 \times 10^{16} \text{ cm}^{-3}$. Consequently, the presence of $\text{C}(^1\text{D})$ atoms in the flow are not expected to affect

any of the present kinetic measurements. Considering the experimental conditions employed, the C(³P) fluorescence signal decays exponentially to zero as a function of time, as shown in Figure 3.

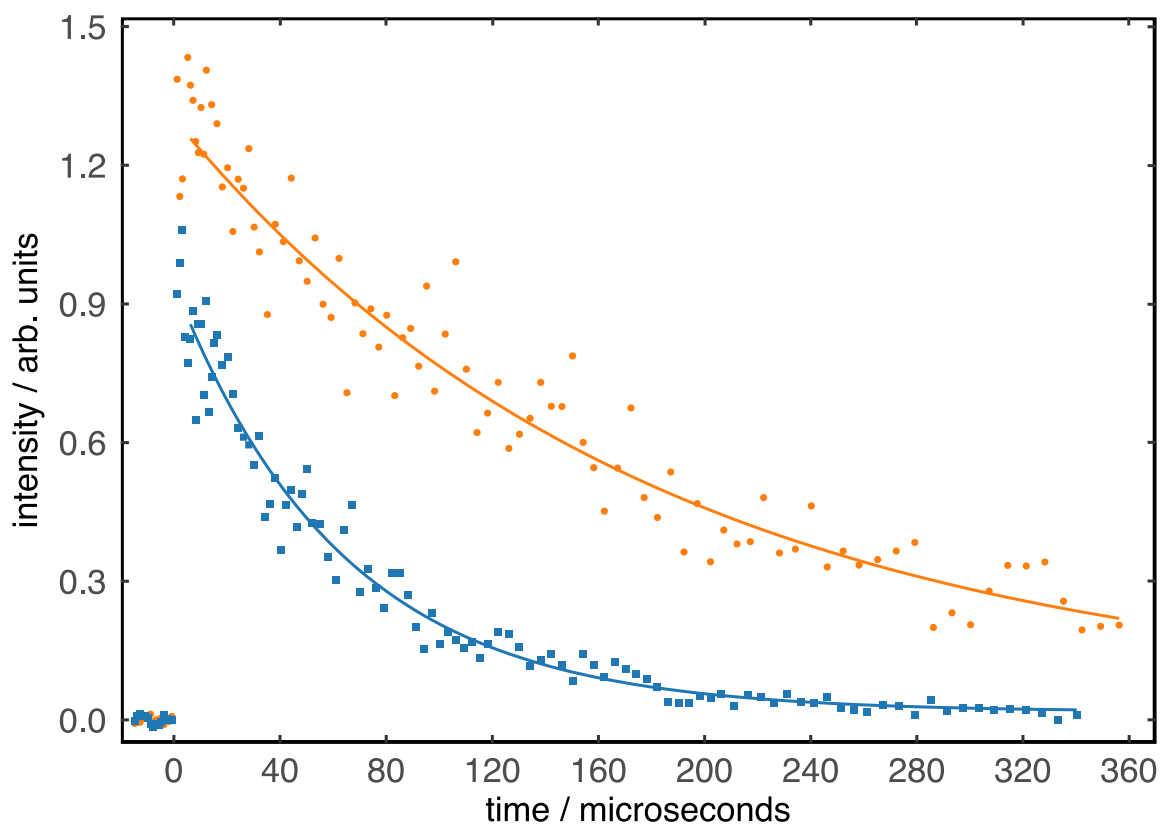


Figure 3 C(³P) fluorescence intensity as a function of delay time recorded at 50 K. (Orange circles) without CH₃COCH₃; (blue squares) [CH₃COCH₃] = 4.6 × 10¹³ cm⁻³. Solid lines represent the non-linear least squares exponential fits to the individual datasets.

These decay curves were well-described by an expression of the form

$$I(t) = I_0 \exp(-k_{1st}t) \quad (1)$$

where I_0 is the C(³P) fluorescence signal intensity at time zero, $I(t)$ is the C(³P) fluorescence signal intensity at time t , and k_{1st} is the pseudo-first-order rate constant for atomic carbon

loss with units s^{-1} . Figure 1 shows that even in the absence of acetone (orange datapoints), the $C(^3P)$ signal decays exponentially. This occurs due to the physical loss of C-atoms through diffusion out of the zone illuminated by the probe laser (diffusional losses, k_{diff}) and by chemical losses such as through the reaction of C-atoms with the precursor molecule CBr_4 ($k_{C+CBr_4}[CBr_4]$) while the loss rate increases considerably when acetone is present in the flow (blue datapoints) due to the additional contribution of the $C + CH_3COCH_3$ reaction ($k_{C+CH_3COCH_3}[CH_3COCH_3]$). As k_{diff} and $k_{C+CBr_4}[CBr_4]$ are constant for any single series of experiments measuring pseudo-first-order decay rates over a range of $[CH_3COCH_3]$, a plot of k_{1st} as a function of $[CH_3COCH_3]$ yields the second-order rate constant $k_{C+CH_3COCH_3}$ for that experiment with units $cm^3 s^{-1}$. The individual datapoints were weighted by the uncertainty derived during the non-linear least squares fitting procedure used to obtain the first order rate constants, according to the expression $w = 1/\sigma^2$ (w is the weight, σ is the uncertainty) so that the data points with the largest associated uncertainty carried the least weight. Several of these second-order plots recorded at different temperatures over the 50-296 K range can be seen in Figure 4.

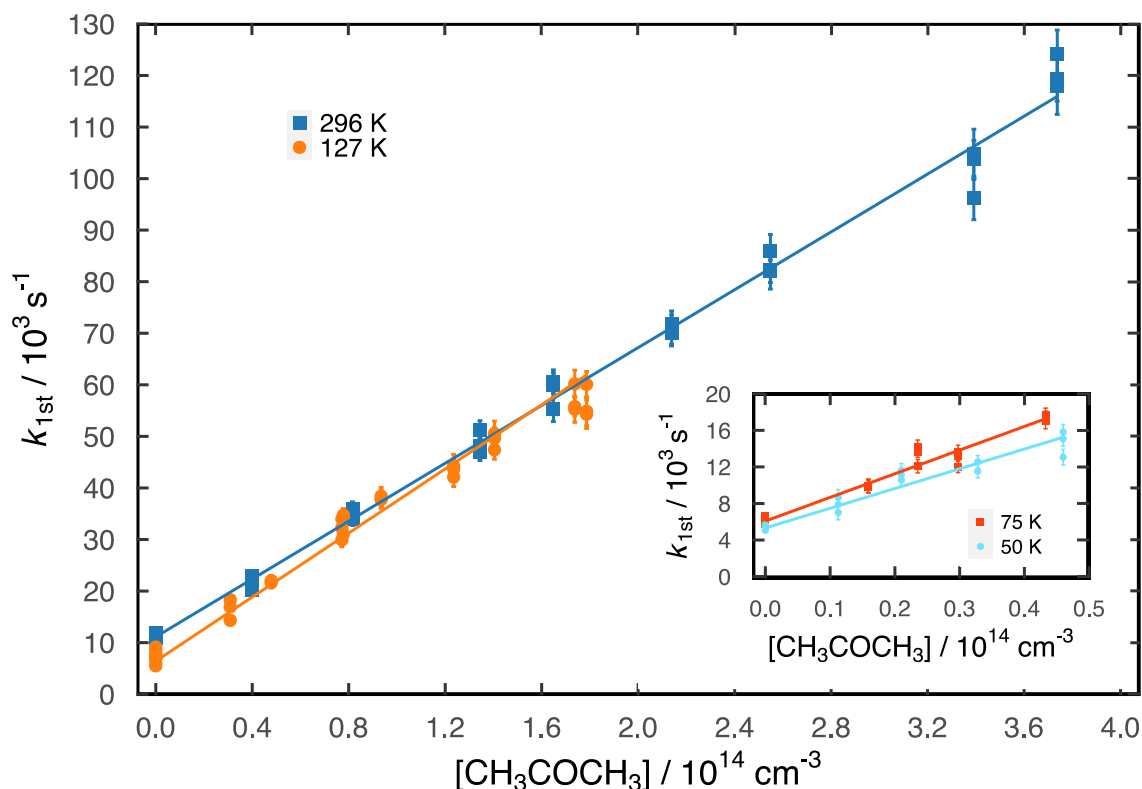


Figure 4 Pseudo-first-order rate constants for atomic carbon loss as a function of the acetone concentration. (Dark blue squares) data recorded at 296 K; (orange circles) data recorded at 127 K. **Inset** (red squares) data recorded at 75 K; (light blue circles) data recorded at 50 K. Solid lines represent weighted linear least-squares fits to the data. Error bars represent the uncertainties on individual pseudo-first-order rate constants derived from non-linear fits to the atomic carbon fluorescence profiles such as those shown in Figure 3.

At least five different concentration values were used to derive the second-order rate constants at any single temperature, based on a minimum of 17 datapoints. The intercept values of these plots at the abscissa correspond to the sum of the $k_{diff} + k_{C+CBr_4}[CBr_4]$ contributions to the k_{1st} values. At the lowest temperatures (50 and 75 K), the derived k_{1st} values only varied linearly as a function of the acetone concentration over a limited range.

Beyond these limiting values, k_{1st} was seen to increase more slowly as the CH_3COCH_3 concentration increased. This observation was considered to be a sign of acetone cluster formation within the cold supersonic flow, effectively preventing a fraction of the acetone monomers from reacting with atomic carbon and lowering the expected pseudo-first-order rate constant. Additionally, the reaction between $\text{C}(^3\text{P})$ and acetone dimers, trimers, etc... may not occur at the same rate as the equivalent monomer reaction and/or lead to alternative reaction pathways. Consequently, only those experiments employing $[\text{CH}_3\text{COCH}_3] < 5 \times 10^{13} \text{ cm}^{-3}$ were used in the final analysis for measurements recorded at 50 and 75 K. The derived second-order rate constants are summarized in Table 1 alongside other relevant information such as the number of measurements and the concentration ranges used.

Table 1 Measured second-order rate constants for the $\text{C}(^3\text{P}) + \text{CH}_3\text{COCH}_3$ reaction

T / K	N^b	$[\text{CH}_3\text{COCH}_3]$ / 10^{13} cm^{-3}	Flow density] / 10^{17} cm^{-3}	$k_{\text{C}(^3\text{P})+\text{CH}_3\text{COCH}_3}$ / $10^{-10} \text{ cm}^3 \text{ s}^{-1}$	Carrier gas
296	30	0 - 37.4	1.65	$(2.81 \pm 0.28)^c$	Ar
177 ± 2^a	30	0 - 12.9	0.94	(2.72 ± 0.28)	N_2
127 ± 2	36	0 - 17.9	1.26	(3.11 ± 0.32)	Ar
75 ± 2	18	0 - 4.3	1.47	(2.59 ± 0.28)	Ar
50 ± 1	17	0 - 4.6	2.59	(2.16 ± 0.24)	Ar

^aUncertainties on the calculated temperatures represent the statistical (1σ) errors obtained from Pitot tube measurements of the impact pressure. ^bNumber of individual measurements. ^cUncertainties on the measured rate constants represent the combined statistical (1σ) and estimated systematic errors (10%).

These values as well as those determined in earlier work are displayed as a function of temperature in Figure 5.

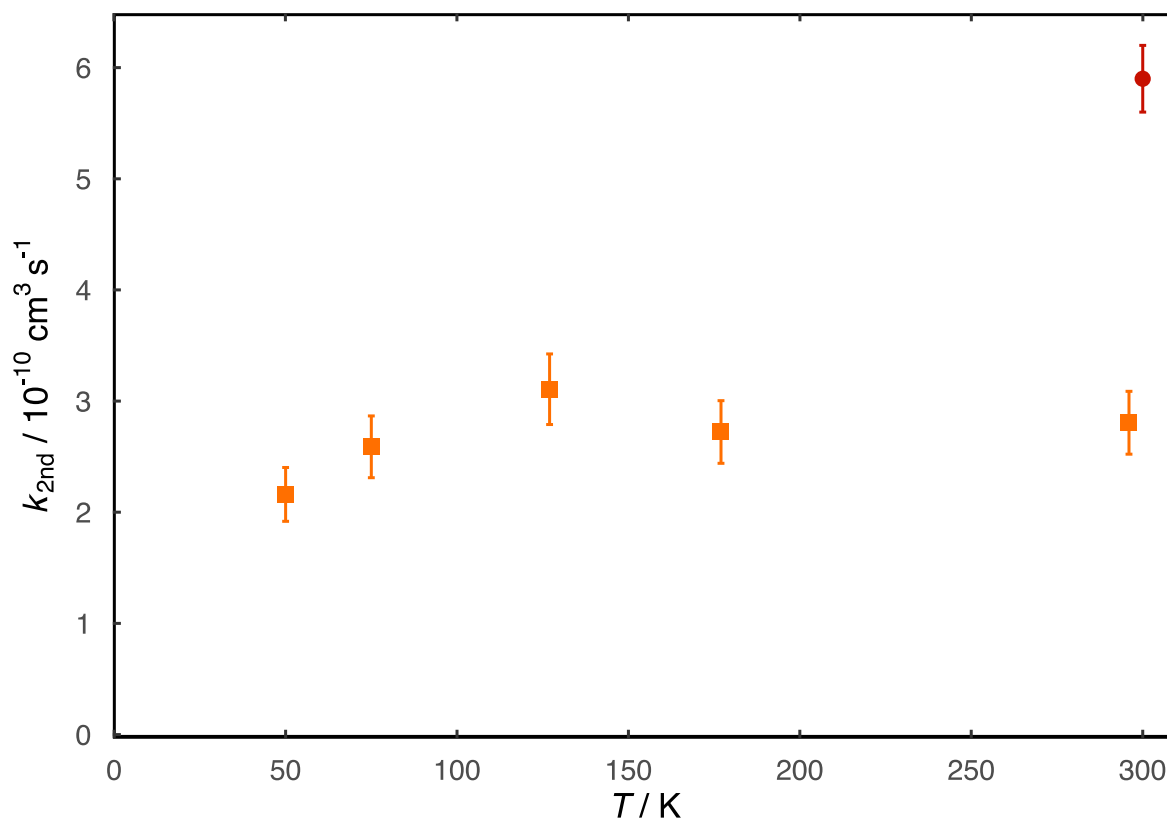


Figure 5 Rate constants for the C + CH₃COCH₃ reaction as a function of temperature. (Red circles) Husain and Ioannou;⁴⁸ (orange squares) this work. Error bars on the present values represent the combined statistical and systematic uncertainties. Statistical uncertainties were derived from weighted linear-least squares fits to the pseudo-first-order rate constants plotted as a function of the acetone concentration as shown in Figure 4. Systematic uncertainties were estimated to be 10 % of the nominal value of the second-order rate constant.

The measured room temperature rate constant is large, with a value $k_{\text{C}+\text{CH}_3\text{COCH}_3}(296\text{ K}) = (2.81 \pm 0.28) \times 10^{-10} \text{ cm}^3 \text{ s}^{-1}$ that is consistent with the presence of at least one barrierless pathway for the C + CH₃COCH₃ reaction. The only other previous kinetic study of the C + CH₃COCH₃ reaction was performed at room temperature by Husain and Ioannou,⁴⁸ who derived a rate constant $k_{\text{C}+\text{CH}_3\text{COCH}_3}(300\text{ K}) = (5.9 \pm 0.3) \times 10^{-10} \text{ cm}^3 \text{ s}^{-1}$; a value more than twice as large as the value derived here at room temperature. Husain and Ioannou⁴⁸ used a conventional flash photolysis apparatus to study this process. In their work, C(³P) atoms were formed by the VUV photolysis ($\lambda > 160 \text{ nm}$) of carbon suboxide, C₃O₂, using a coaxial lamp. Previous work has demonstrated that the major photolysis product in this wavelength range is ground state C(³P) atoms rather than excited state C(¹D) atoms (97 % and 3 % respectively) so that relaxation of C(¹D) atoms back to the ground state was expected to be essentially negligible during this work. C(³P) atoms were followed by absorption, using the emission from an atomic resonance lamp at 166 nm, optically isolated using a VUV monochromator and a solar blind PMT. The large difference in rate constant values between the present work and this previous study is difficult to understand. Nevertheless, it is clear that the use of an absorption-based detection method (as opposed to the fluorescence-based method used here) requires the use of much larger C(³P) concentrations for equivalent signal-to-noise ratios, potentially leading to higher levels of secondary reactions. Moreover, as the C-atom precursor C₃O₂ has a very large absorption cross-section around 166 nm ($\sim 1 \times 10^{-16} \text{ cm}^2$), any concentration changes of this species during the course of a single experiment (such as through depletion by the repetitive photolysis technique employed by Husain and Ioannou⁴⁸) would alter the transmitted signal levels leading to an incorrect decay profile. As the C-atom precursor molecule used in our study (CBr₄) has an absorption cross-section at 266 nm that is

a hundred times smaller than the C_3O_2 cross-section at 166 nm, the equivalent issue should not arise in the present work.

The measured rate constants show only small variations as a function of temperature, with values of $(2.1-3.1) \times 10^{-10} \text{ cm}^3 \text{ s}^{-1}$ over the 50-296 K range. The absence of a strong temperature dependence of the rate constant would seem to indicate that the major pathways are not strongly influenced by the presence of a pre-reactive complex in the entrance channel. Indeed, earlier studies of the barrierless reactions of $C(^3P)$ with other reagents involving complex formation and a submerged barrier towards adduct formation^{5, 14, 31} present much stronger temperature dependences than those C-atom reactions where these features are absent.¹⁵ Despite this, the measured reaction rates at 75 and 50 K are slightly lower than those obtained at higher temperature, although the differences are close to being covered by the combined measurement uncertainties. In this respect, for low temperature interstellar modelling purposes, we recommend the use of a temperature independent value for the rate constant, $k_{C+CH_3COCH_3} = 2.2 \times 10^{-10} \text{ cm}^3 \text{ s}^{-1}$. Mechanistically, the observed rate constant decrease could be indicative of the opening of the reactive channel via TS2 as the temperature falls (see Figure 1), with part of the reactive flux being trapped in MIN2 rather than passing by the other barrierless channels via MIN1 and MIN9. Further evidence for the opening of this channel will be presented in section 4.3.

4.3 Temperature dependent H-atom yields

The measurement of H-atom VUV LIF intensities at 75, 177 and 296 K allowed us to gain some insight into the H-atom forming product channels of the $C + CH_3COCH_3$ reaction. In order to put these measurements on an absolute scale, the derived intensity was compared to the one recorded for a reference process. In this case, the $C + C_2H_4 \rightarrow C_3H_3 + H$ reaction, with a

measured H-atom yield of 0.92 ± 0.04 at 300 K,⁴⁹ was used to calibrate the H-atom yield of the $C + CH_3COCH_3$ reaction. We assume that this yield does not change over the present temperature range due to the absence of a prereactive complex for this process coupled with the absence of any significant (submerged) barriers over the triplet PES leading to $C_3H_3 + H$ products.⁵⁰ As $C(^1D)$ atoms were also present in the supersonic flow during these experiments, it was necessary to check that the production of any additional H-atoms by the reactions of $C(^1D)$ with both CH_3COCH_3 and C_2H_4 did not interfere with our measurements of the equivalent ground state processes. These checks were performed by replacing all (or part) of the carrier gas Ar by N_2 in some experiments, as N_2 is known to quench $C(^1D)$ atoms much more rapidly than Ar, with a quenching rate constant that increases as the temperature falls.³² In this respect, experiments were carried out at 296 K using both Ar and N_2 as the carrier gases, while a large concentration of N_2 ($1.5 \times 10^{16} \text{ cm}^{-3}$) was added to the flow during measurements performed at 75 K. The carrier gas used to produce supersonic flows at 177 K is N_2 , so no additional checks were required for these measurements.

Unfortunately, as can be seen from Figure 6, recorded at 75 K, the present experiments were hampered by the production of atomic hydrogen from the photolysis of acetone at 266 nm which added to the H-atom signal produced by the $C + CH_3COCH_3$ reaction.

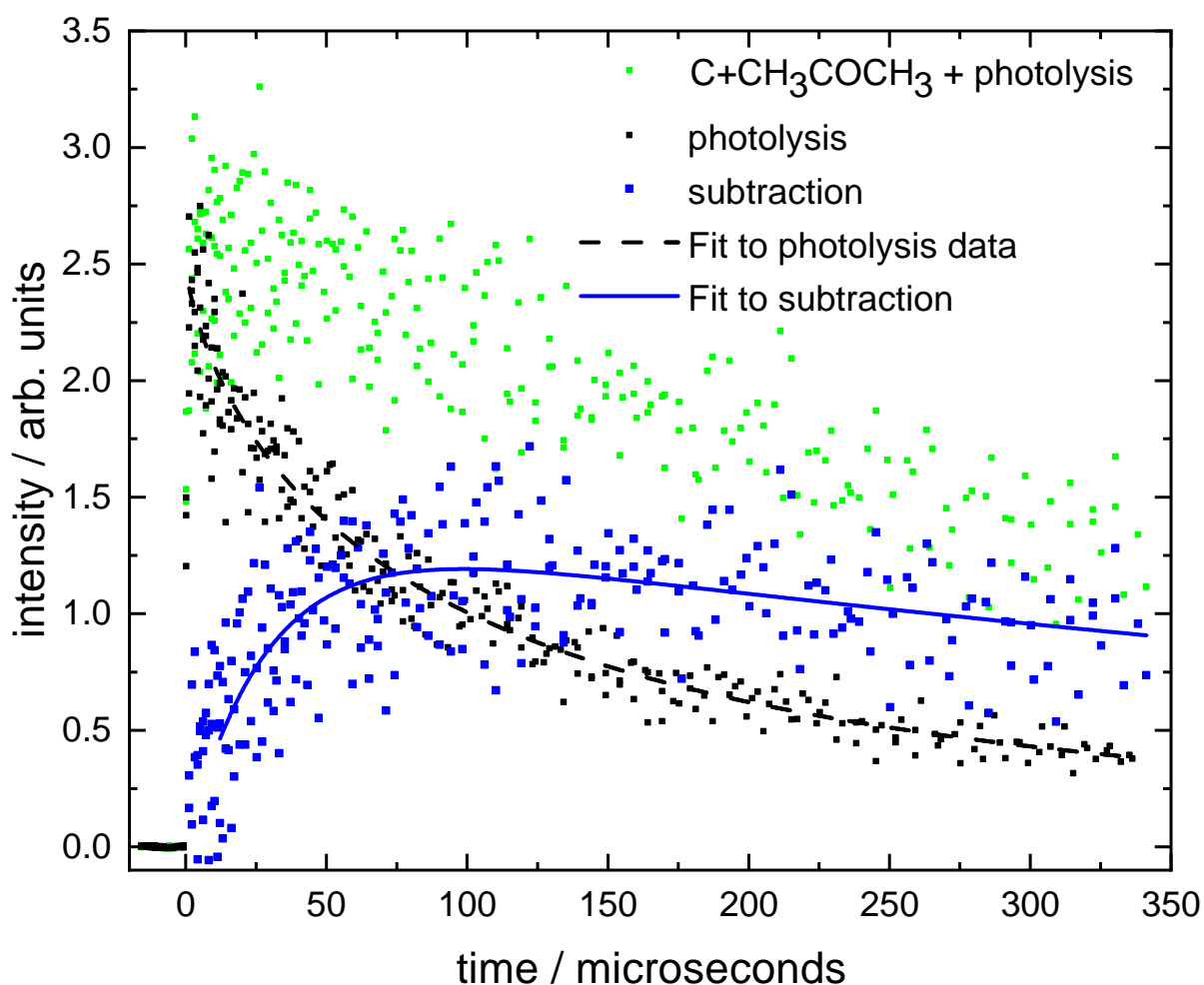


Figure 6 Recorded H-atom signals as a function of time at 75 K. (Solid green squares) H-atom signal produced by CH_3COCH_3 photolysis and the $\text{C} + \text{CH}_3\text{COCH}_3$ reaction. (Solid black squares) H-atom signal produced by CH_3COCH_3 photolysis alone (no CBr_4 was present in the flow). (Dashed black line) fit to the CH_3COCH_3 photolysis data. (Solid blue squares) subtraction of the photolysis contribution from the green datapoints, representing the reactive H-atom signal. (Solid blue line) biexponential fit to the reactive H-atom signal.

In order to extract the contribution from the $\text{C} + \text{CH}_3\text{COCH}_3$ reaction alone, two different experiments were performed. Firstly, the H-atom temporal signal was recorded with the photolysis laser on, with both atomic carbon and CH_3COCH_3 present in the supersonic flow to yield the sum of the two contributions (reaction + photolysis - green points in Figure 6). Then,

a second experiment was performed where the vessel containing CBr₄ was isolated from the supersonic flow. Under these conditions, no C-atoms are present in the flow so that only the H-atom signal from acetone photolysis is recorded (black points in Figure 6). This procedure is repeated at least 3 or 4 times and the resulting curves of the same type are coadded and analyzed. This method was preferred over the one used in previous work, where pairs of curves (target reaction followed by reference reaction or vice-versa) were recorded and analyzed separately, due to the larger uncertainty of the present work brought about by the requirement to subtract the H-atom signal generated by photolysis. Indeed, Figure 6 above recorded at 75 K shows the results of three coadded temporal curves of each type (photolysis+reaction and photolysis alone).

An arbitrary function is chosen to produce a good fit to the photolysis data, which is then subtracted from the trace containing the photolysis+reactive contribution to leave the reactive contribution alone (blue points in Figure 6). It can be seen that these data have the biexponential form expected for a production process in Laval nozzle flows (H-atom formation followed by its diffusional loss). Consequently, these data were well described by the following expression

$$I_H = A\{\exp(-k_{L(H)}t) - \exp(-k_{1st}t)\} \quad (2)$$

to yield the blue line shown in Figure 6. Here, I_H is the H-atom signal intensity and $k_{L(H)}$ represents the secondary H-atom loss through processes such as diffusion. These data are then compared to the H-atom signal produced by the C + C₂H₄ reference reaction as shown in Figure 7 for two different temperatures (upper panel - 296 K, lower panel - 75 K).

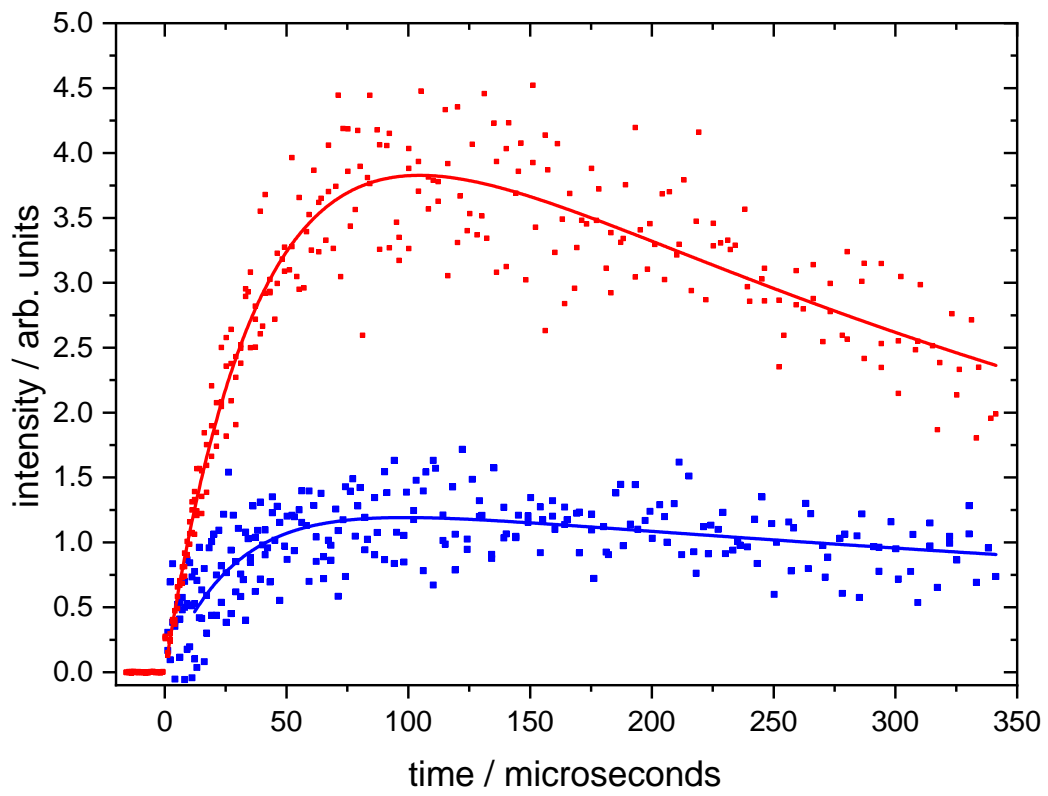
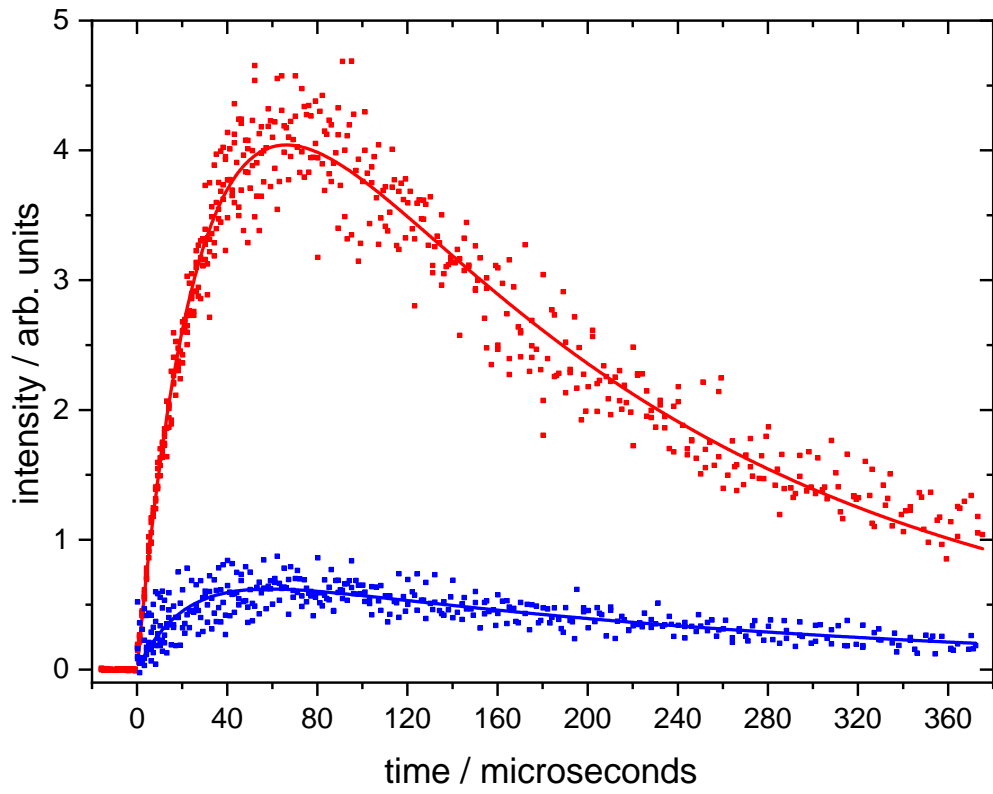


Figure 7 (Upper panel) H-atom formation curves recorded at 296 K. (red solid squares) H-atom formation by the C + C₂H₄ reaction ([C₂H₄] = 4.3 × 10¹³ cm⁻³). (Blue solid squares) H-atom formation by the C + CH₃COCH₃ reaction ([CH₃COCH₃] = 2.4 × 10¹³ cm⁻³) resulting from the subtraction procedure described in the text and displayed in Figure 6. (Lower panel) H-atom formation curves recorded at 75 K. (red solid squares) H-atom formation by the C + C₂H₄ reaction ([C₂H₄] = 1.5 × 10¹³ cm⁻³). (Blue solid squares) H-atom formation by the C + CH₃COCH₃ reaction ([CH₃COCH₃] = 1.7 × 10¹³ cm⁻³) resulting from the subtraction procedure described in the text and displayed in Figure 6. Solid red and blue lines represent biexponential fits to the subtracted data.

To be consistent with the data for the C + CH₃COCH₃ target reaction, all H-atom temporal curves for the C + C₂H₄ reference reaction were also co-added before analysis. The peak intensities of the H-atom formation curves for the C + C₂H₄ reference reaction shown in Figure 7 were then divided by 0.92 to correct for the fact that the measured H-atom yields for this process are slightly smaller than 1.⁴⁹ Absolute H-atom yields for the C(³P) + CH₃COCH₃ reaction were then obtained by dividing the peak values from the fitted curves for the C(³P) + CH₃COCH₃ reaction by the corrected peak values for the C(³P) + C₂H₄ reaction. No further corrections were required in the present experiments as the low CH₃COCH₃ and C₂H₄ concentrations used here were estimated to result in less than 1 % absorption losses at 121.567 nm. The derived absolute H-atom yields for the C(³P) + CH₃COCH₃ reaction are listed in Table 2.

Table 2 H atom yields for the C(³P) + CH₃COCH₃ reaction as a function of temperature

T / K	Number of experiments	H atom yield
296	12	0.13 ± 0.02
177	7	0.25 ± 0.04
75	8	0.29 ± 0.03

^aThe error bars reflect the statistical uncertainties at the level of a single standard deviation including the uncertainties of the H branching ratio of the C + C₂H₄ reaction used as a reference with a systematic error of 10 % added to account for the higher uncertainty brought about by the subtraction procedure described above.

It can be clearly seen from Figure 7 and Table 2 that the H-atom yield of the C + CH₃COCH₃ reaction becomes more important, relative to the yield of the C + C₂H₄ reaction, at low temperature although H-atom formation pathways are minor channels at all temperatures.

Considering the exothermicity of MIN1 followed by the direct dissociative pathway to products P9, it is likely that this represents the major exit channel of the C + CH₃COCH₃ reaction at room temperature and below. Nevertheless, we cannot exclude the transitory formation of MIN3, given the low value of TS1 and the high exothermicity of MIN3. We would then expect that MIN3 dissociates to the most thermodynamically stable products P9 through C-C bond fission although several other channels such as the ones towards P7 (H + CH₂CCOCH₃) through C-H bond fission and P8 (CH₃ + CH₃CCO) through C-C fission, and the isomerization pathway towards MIN6 and eventually P6 (HCO + CH₃CCH₂) are also energetically accessible so these cannot be excluded. The pathways MIN9→TS11→MIN8→TS4→MIN3 and MIN9→TS13→P9 might also play a role in the reaction. TS13 is 161 kJ/mol below the reagent level, so this latter pathway should not present any temperature dependence. Although TS11 is only 91 kJ/mol below the reagents, it also

seems unlikely that this would be high enough to lead to significant temperature dependent effects in the former pathway. The main predicted pathways of the C + CH₃COCH₃ reaction (that is via MIN1→P9 and MIN1→MIN3→P9) do not present any substantial barriers (or submerged barriers) to product formation. As the temperature falls it is expected that the lifetime of MIN3 will increase which might favour the formation of products other than CH₃CCH₃ + CO. Indeed, as no TS was located along the dissociation pathway MIN3→P7 (CH₂CCOCH₃+H), this pathway may represent a minor exit channel producing H-atoms. Similarly, the pathways MIN3 → MIN6 → P6(HCO+CH₃CCH₂) → P4(H+CO+CH₃CCH₂) and MIN3 → MIN6 → P6(HCO+CH₃CCH₂) → P3(H+HCO+H₂CCCH₂) could also be sources of H-atoms as both HCO and CH₃CCH₂ dissociation to H + CO and H + H₂CCCH₂ respectively are energetically accessible exit channels. To test for the possibility of HCO dissociation to H + CO, experiments were conducted at room temperature with two different densities of N₂ carrier gas (1.6 and 3.2 × 10¹⁷ cm⁻³). According to the study by Langford and Moore,⁵¹ the vibrational relaxation process HCO(0,1,0) + N₂ → HCO(0,0,0) + N₂ is characterized by a rate constant of 2.5 × 10⁻¹³ cm³ s⁻¹ leading to pseudo-first-order decay rates of 4 and 8 × 10⁴ s⁻¹. Earlier studies of the unimolecular dissociation of HCO over a range of pressures and temperatures⁵² indicate that this process is likely to be an order of magnitude slower (a few 10³ s⁻¹) so if H-atoms were produced predominantly by this mechanism we would expect to see a notable difference in the H-atom yields as a function of pressure. The H-atom yields derived by these two experiments were almost identical (0.13 at lower pressure compared with 0.14 at higher pressure), indicating that H-atom formation by HCO dissociation is likely to be a minor contribution overall.

Alternatively, the pathway MIN2→MIN4→P5 might become more important as the temperature falls, even though the energies calculated at the DLPNO-CCSD(T)/AVTZ energies

are close to the reagent level. Here, the formation of the weakly bound van der Waals type complex MIN2 (-1 kJ/mol at the DLPNO-CCSD(T)/AVTZ level corrected for ZPE) should become more favorable at low temperature, diverting a fraction of the reactive flux away from the major pathways described above. As TS2 is also low (0 kJ/mol at the DLPNO-CCSD(T)/AVTZ level corrected for ZPE), the production of P5 (H + HCCHCOCH₃) via MIN4 could explain the observed increase in H-atom production as the temperature falls. In order to validate this hypothesis, additional electronic structure calculations should be performed at a higher level of theory (such as by using double-hybrid DFT or wavefunction based methods for the geometry optimization steps and/or larger basis sets) coupled with statistical RRKM type calculations to provide further interpretation of the experimental data, with H-atom formation potentially arising from several different product channels (MIN3→MIN6→P6→P4, MIN3→MIN6→P6→P3, MIN3→P7, MIN2→MIN4→P5). Nevertheless, if the barrier height TS2 for the channel MIN2→MIN4→P5 is submerged with respect to the reagent level, this pathway represents a plausible explanation for the observed increased H-atom yield at lower temperature. As an alternative possibility, as mentioned above, the longer expected lifetime of MIN3 as the temperature falls could also favour the production of H-atoms through the H + CH₂CCOCH₃ exit channel (P7).

5 Astrochemical Model and Comparison with Observations

Considering the absence of the C + CH₃COCH₃ reaction in astrochemical databases such as KIDA,²² it is interesting to test the effect of this process on the abundances of CH₃COCH₃ and other related species predicted by astrochemical models. Here, we used the gas-grain model Nautilus^{53, 54} in its three-phase form^{55, 56} to simulate the abundances of atoms and molecules in neutral and ionic form as a function of time, employing kida.uva.2014²² as the basic

reaction network updated recently for a better description of COMs on grains and in the gas-phase.^{18, 57, 58} 800 individual species are included in the network that are involved in 9000 separate reactions. Elements are either initially in their atomic or ionic forms in this model (elements with an ionization potential < 13.6 eV are considered to be fully ionized) and the C/O elemental ratio is equal to 0.71 in this work. The initial simulation parameters are listed in Table 3.

Table 3 Elemental abundances and other model parameters

Element	Abundance ^(a)	$n\text{H} + 2n\text{H}_2 / \text{cm}^{-3}$	T/ K	Cosmic ray ionization rate / s^{-1}	Visual extinction
H ₂	0.5	2.5×10^4	10	1.3×10^{-17}	10
He	0.09				
C ⁺	1.7×10^{-4}				
N	6.2×10^{-5}				
O	2.4×10^{-4}				
S ⁺	1.5×10^{-5}				
Fe ⁺	3.0×10^{-9}				
Cl ⁺	1.0×10^{-9}				
F	6.7×10^{-9}				

^(a)Relative to total hydrogen ($n\text{H} + 2n\text{H}_2$)

The grain surface and the mantle are both chemically active for these simulations, while accretion and desorption are only allowed between the surface and the gas-phase. The dust-to-gas ratio (in terms of mass) is 0.01. A sticking probability of 1 is assumed for all neutral species while desorption can occur by thermal and non-thermal processes (cosmic rays, chemical desorption) including sputtering of ices by cosmic-ray collisions.⁵⁹ The surface reactions formalism and a more detailed description of the simulations can be found in Ruaud et al.⁵⁵

A large fraction of the CH₃COCH₃ present in our updated model¹⁸ originates from the reactions of the C₃ species. Here, the C₃ + H₃⁺ reaction, followed by a sequence of hydrogen transfers with H₂ lead eventually to the formation of C₃H₅⁺ and C₃H₇⁺. Then, the OH + C₃H₇⁺

and $\text{H}_2\text{O} + \text{C}_3\text{H}_5^+$ reactions produce $\text{CH}_3\text{COHCH}_3^+$ (with a secondary contribution from the $\text{C}_2\text{H}_4 + \text{H}_2\text{COH}^+$ reaction) which undergoes electronic Dissociative Recombination (DR) to yield CH_3COCH_3 .

The neutral $\text{O} + 2\text{-C}_3\text{H}_7$ ($\text{CH}_3\text{-CH-CH}_3$) reaction,⁶⁰ where 2-C₃H₇ itself is produced on grains, is also a minor but non-negligible route for producing CH_3COCH_3 . The main losses of gas-phase CH_3COCH_3 are through reaction with H_3^+ and HCO^+ , through reaction with atomic C (this work) and the OH radical,^{25, 61} and by depletion onto grains.

As can be seen from Figure 8, introduction of the $\text{C} + \text{CH}_3\text{COCH}_3$ reaction into the network with an estimated rate constant, $k_{\text{C}+\text{CH}_3\text{COCH}_3}(10\text{ K}) = 2.2 \times 10^{-10} \text{ cm}^3 \text{ s}^{-1}$, leads to a maximum decrease of the CH_3COCH_3 abundance of up to two orders of magnitude between 10^3 and 10^5 years. For the present test, we chose to limit product formation to the $\text{C}_3\text{H}_6 + \text{CO}$ channel as the possible $\text{C}_4\text{H}_5\text{O}$ product isomers in particular are not currently included in the model.

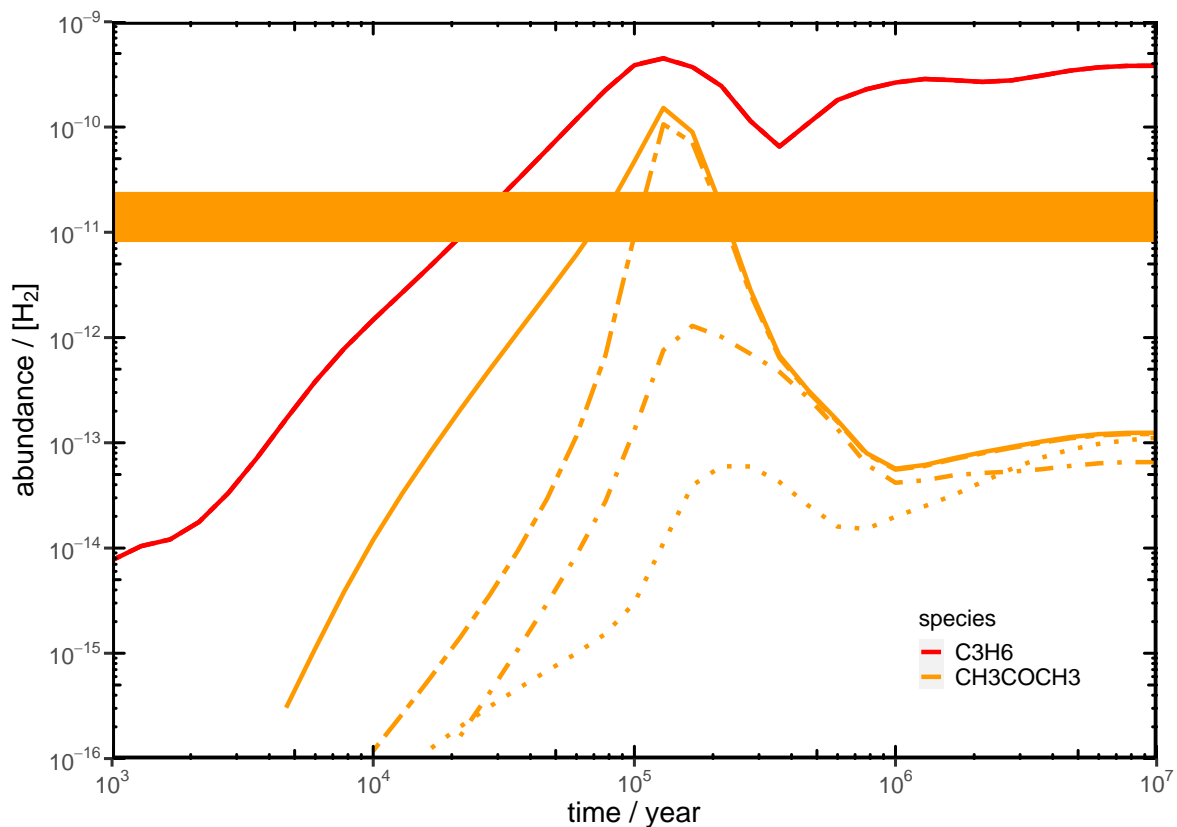


Figure 8 Gas-grain astrochemical model results for the formation of CH₃COCH₃ (orange lines) and C₃H₆ (red lines) in dark clouds as a function of cloud age. (Solid line) standard network results. (Short dashed - long dashed line) the same network but with the gas-phase C + CH₃COCH₃ reaction included. (Dashed-dotted line) new network without the I-C₃H₃⁺ + H₂ and C₃H₅⁺ + H₂ reactions. (Dotted line) new network with the rate constant of the gas-phase O + C₃ reaction set to $1 \times 10^{-11} \text{ cm}^3 \text{ s}^{-1}$. The C₃H₆ abundances given by the standard network (Red solid line) and the network including the C + CH₃COCH₃ reaction (Red short dashed - long dashed line) are indistinguishable on the present scale. The horizontal orange rectangle represents the observed CH₃COCH₃ abundance in TMC-1¹⁸ with an arbitrary error associated ($\pm\sqrt{3}$).

At ages considered to be characteristic of typical dense clouds (a few 10^5 years), atomic carbon is removed from the gas-phase through gas-phase reactions forming CO and by accretion onto grains, thereby limiting the effect of the $C + CH_3COCH_3$ reaction at longer times ($>10^5$ years). Despite the effect of the $C + CH_3COCH_3$ reaction on CH_3COCH_3 abundances at early times, these simulations indicate that the $C + CH_3COCH_3$ reaction induces only small changes in the gas-phase abundance of CH_3COCH_3 at typical dense interstellar cloud ages, with a calculated CH_3COCH_3 abundance in good agreement with the observations for TMC-1¹⁸ at ages considered to be characteristic of typical dense clouds (a few 10^5 years). As C_3H_6 is the expected major product of the $C + CH_3COCH_3$ reaction, the predicted C_3H_6 abundances for our standard network and for the network including the $C + CH_3COCH_3$ reaction are displayed in red in Figure 8. These two curves essentially overlap, indicating that the title reaction is only a very minor source of gas-phase propene in this model. The major source of C_3H_6 in our simulations is the $C_3H_7^+ + e^-$ DR reaction.

As discussed above, according to our updated network, the chemistry of acetone in dense clouds is strongly linked to the chemistry of C_3 , which provides the C_3 backbone for this molecule. The agreement between the observations and the simulations for CH_3COCH_3 is therefore highly dependent on the efficiency of the $O + C_3$ reaction, for which the calculations by Woon and Herbst⁶² predict a barrier in the entrance channel, leading to a negligible reaction rate at 10 K. This agreement is also highly dependent on the rates of the reactions of $C_3H_3^+$ and $C_3H_5^+$ with H_2 which are very slow at room temperature⁶³ but which can be non-negligible at low temperature⁶⁴ due to tunneling. The effects of changing the reactivities of C_3 with atomic oxygen, and of $C_3H_3^+$ and $C_3H_5^+$ with H_2 are shown in Figure 8. If C_3 is allowed to react with atomic oxygen at 10 K, CH_3COCH_3 is largely underestimated in the model. However, if O and C_3 are unreactive at low temperature, it allows the observed CH_3COCH_3

abundance in dense molecular clouds to be reproduced but induces a high abundance of C_3 in the gas-phase which seems to be incompatible with the ^{13}C fractionation of $c-C_3H_2$ ⁶⁵ and with the observed abundances of CH_3CCH and C_3H_6 in protostars.⁵⁷ If the rates of the reactions of $C_3H_3^+$ and $C_3H_5^+$ with H_2 are negligible at 10 K, the model significantly underestimates the CH_3COCH_3 abundance as these processes control the abundances of $C_3H_5^+$ and $C_3H_7^+$ which are important species for the production of CH_3COCH_3 . In parallel, these hydrogenation reactions also allow the model to reproduce the observations of CH_3CCH ⁶⁶ and C_3H_6 ,⁶⁷ which models struggle to reproduce otherwise.⁶⁸ It should also be noted that in addition to CH_3CCH , C_3H_6 and CH_3COCH_3 , the reactions of $C_3H_3^+$ and $C_3H_5^+$ with H_2 also control the production of several other species including CH_3CHO , produced mainly by the $O + C_2H_5$ reaction. CH_3CHO is largely underestimated in the models if C_3H_6 is also underestimated because the main source of C_2H_5 radicals in dense molecular cloud networks is the $O + C_3H_6$ reaction.^{69,70} Clearly, considering the number of species affected by the $O + C_3$ reaction and the reactions of $C_3H_3^+$ and $C_3H_5^+$ with H_2 , including CH_3COCH_3 , CH_3CHO , CH_3CCH and C_3H_6 , it is particularly important to provide better constraints for the rates of these reactions at low temperatures.

6 Conclusions

This study reports the results of a combined experimental/theoretical/astrochemical modeling investigation of the $C(^3P) + CH_3COCH_3$ reaction. Experiments were performed using an existing supersonic flow reactor coupled with pulsed laser photolysis and pulsed laser induced fluorescence for the detection of $C(^3P)$ and $H(^2S)$ at vacuum ultraviolet wavelengths to obtain temperature dependent rate constants over the 50-296 K temperature range and temperature dependent branching ratios for H-atom formation over the 75-296 K range. Electronic structure calculations clearly show the barrierless nature of the pathways leading

to ${}^3\text{C}_3\text{H}_6 + \text{CO}$ as the major products at all temperatures, with further evolution of ${}^3\text{C}_3\text{H}_6$ to ground state ${}^1\text{C}_3\text{H}_6$ predicted to occur through intersystem crossing. Several minor channels ($\text{CH}_2\text{CCOCH}_3 + \text{H}$, $\text{CH}_3\text{CCH}_2 + \text{H} + \text{CO}$, $\text{C}_3\text{H}_4 + \text{HCO} + \text{H}$) could be responsible for the production of a large fraction of the H-atoms observed experimentally. The presence of a weakly bound van der Waals complex between C and CH_3COCH_3 might explain the observed temperature dependence of the H-atom yield, through an increased production of $\text{H} + \text{HCCHCOCH}_3$ as the temperature falls. Further experiments and/or theoretical work will be required to disentangle the relative contributions of these pathways. The effect of the $\text{C}({}^3\text{P}) + \text{CH}_3\text{COCH}_3$ reaction on interstellar acetone abundances was tested through a gas-grain dense interstellar cloud model. Using a temperature independent rate constant value of $2.2 \times 10^{-10} \text{ cm}^3 \text{ s}^{-1}$, the simulations showed that the gas-phase acetone abundance decreased by as much as two orders of magnitude at early times, with only a small reduction in the acetone abundance at cloud ages considered to be representative of dense interstellar clouds. Despite its high reactivity, the $\text{C}({}^3\text{P}) + \text{CH}_3\text{COCH}_3$ reaction is predicted to be only a minor source of propene in this model.

Author Information

Corresponding Author

*Email: kevin.hickson@u-bordeaux.fr.

Supporting Information

Geometries and frequencies of the stationary points involved in the $\text{C}({}^3\text{P}) + \text{CH}_3\text{COCH}_3$ reaction obtained at the M06-2X/aug-cc-pVTZ level of theory (DOCX).

Acknowledgements

K. M. H. and V. W. acknowledge support from the French program “Physique et Chimie du Milieu Interstellaire” (PCMI) of the CNRS/INSU with the INC/INP co-funded by the CEA and CNES. K. M. H. also acknowledges support from the “Programme National de Planétologie” (PNP) of the CNRS/INSU.

References

- (1) Schilke, P.; Keene, J.; Lebourlot, J.; Desforets, G. P.; Roueff, E. Atomic Carbon in a Dark Cloud - TMC-1. *Astron. Astrophys.* **1995**, *294*, L17-L20.
- (2) Ikeda, M.; Maezawa, H.; Ito, T.; Saito, G.; Sekimoto, Y.; Yamamoto, S.; Tatematsu, K.; Arikawa, Y.; Aso, Y.; Noguchi, T.; et al. Large-Scale Mapping Observations of the C I (3P_1 - 3P_0) and CO ($J = 3-2$) Lines Toward the Orion A Molecular Cloud. *Astrophys. J.* **1999**, *527*, L59-L62.
- (3) Ikeda, M.; Oka, T.; Tatematsu, K.; Sekimoto, Y.; Yamamoto, S. The Distribution of Atomic Carbon in the Orion Giant Molecular Cloud 1. *Astrophys. J., Suppl. Ser.* **2002**, *139*, 467.
- (4) Bensch, F. Neutral Carbon and CO Emission in the Core and the Halo of Dark Cloud Barnard 5. *Astron. Astrophys.* **2006**, *448*, 1043-1060.
- (5) Hickson, K. M.; Loison, J.-C.; Larregaray, P.; Bonnet, L.; Wakelam, V. An Experimental and Theoretical Investigation of the Gas-Phase $C(^3P) + N_2O$ Reaction. Low Temperature Rate Constants and Astrochemical Implications. *J. Phys. Chem. A* **2022**, *126*, 940-950.
- (6) Clary, D. C.; Haider, N.; Husain, D.; Kabir, M. Interstellar Carbon Chemistry: Reaction Rates of Neutral Atomic Carbon with Organic Molecules. *Astrophys. J.* **1994**, *422*, 416.
- (7) Clary, D. C.; Buonomo, E.; Sims, I. R.; Smith, I. W. M.; Geppert, W. D.; Naulin, C.; Costes, M.; Cartechini, L.; Casavecchia, P. $C + C_2H_2$: A Key Reaction in Interstellar Chemistry. *J. Phys. Chem. A* **2002**, *106*, 5541-5552.
- (8) Chastaing, D.; James, P. L.; Sims, I. R.; Smith, I. W. M. Neutral-Neutral Reactions at the Temperatures of Interstellar Clouds: Rate Coefficients for Reactions of Atomic Carbon, $C(^3P)$, with O_2 , C_2H_2 , C_2H_4 and C_3H_6 down to 15 K. *Phys. Chem. Chem. Phys.* **1999**, *1*, 2247-2256.
- (9) Chastaing, D.; Le Picard, S. D.; Sims, I. R.; Smith, I. W. M.; Geppert, W. D.; Naulin, C.; Costes, M. Rate Coefficients and Cross-Sections for the Reactions of $C(^3P_j)$ Atoms with Methylacetylene and Allene. *Chem. Phys. Lett.* **2000**, *331*, 170-176.
- (10) Kaiser, R. I.; Mebel, A. M. The Reactivity of Ground-State Carbon Atoms with Unsaturated Hydrocarbons in Combustion Flames and in the Interstellar Medium. *Int. Rev. Phys. Chem.* **2002**, *21*, 307-356.
- (11) Leonori, F.; Petrucci, R.; Segoloni, E.; Bergeat, A.; Hickson, K. M.; Balucani, N.; Casavecchia, P. Unraveling the Dynamics of the $C(^3P, ^1D) + C_2H_2$ Reactions by the Crossed Molecular Beam Scattering Technique. *J. Phys. Chem. A* **2008**, *112*, 1363-1379.
- (12) Costes, M.; Halvick, P.; Hickson, K. M.; Daugey, N.; Naulin, C. Non-Threshold, Threshold, and Nonadiabatic Behavior of the Key Interstellar $C + C_2H_2$ Reaction. *Astrophys. J.* **2009**, *703*, 1179-1187.
- (13) Naulin, C.; Daugey, N.; Hickson, K. M.; Costes, M. Dynamics of the Reactions of $C(^3P_j)$ Atoms with Ethylene, Allene, and Methylacetylene at Low Energy Revealed by Doppler-Fizeau Spectroscopy. *J. Phys. Chem. A* **2009**, *113*, 14447-14457.

- (14) Shannon, R. J.; Cossou, C.; Loison, J.-C.; Caubet, P.; Balucani, N.; Seakins, P. W.; Wakelam, V.; Hickson, K. M. The Fast C(³P) + CH₃OH Reaction as an Efficient Loss Process for Gas-Phase Interstellar Methanol. *RSC Adv.* **2014**, *4*, 26342-26353.
- (15) Hickson, K. M.; Loison, J.-C.; Wakelam, V. Kinetic Study of the Gas-Phase C(³P) + CH₃CN Reaction at Low Temperatures: Rate Constants, H-Atom Product Yields, and Astrochemical Implications. *ACS Earth Space Chem.* **2021**, *5*, 824-833.
- (16) Combes, F.; Gerin, M.; Wootten, A.; Wlodarczak, G.; Clausset, F.; Encrenaz, P. J. Acetone in interstellar Space. *Astron. Astrophys.* **1987**, *180*, L13-L16.
- (17) Snyder, L. E.; Lovas, F. J.; Mehringer, D. M.; Miao, N. Y.; Kuan, Y. J.; Hollis, J. M.; Jewell, P. R. Confirmation of Interstellar Acetone. *Astrophys. J.* **2002**, *578*, 245-255.
- (18) Agúndez, M.; Loison, J. C.; Hickson, K. M.; Wakelam, V.; Fuentetaja, R.; Cabezas, C.; Marcelino, N.; Tercero, B.; de Vicente, P.; Cernicharo, J. Detection of Ethanol, Acetone, and Propanal in TMC-1 New O-bearing Complex Organics in Cold Sources. *Astron. Astrophys.* **2023**, *673*, A34.
- (19) Zou, L.; Widicus Weaver, S. L. Observation and Analysis of Interstellar Acetone in GAL 31.41+0.31, GAL 034.3+00.2, and GAL 10.47+00.03. *Astrophys. J.* **2017**, *849*, 139.
- (20) Lykke, J. M.; Coutens, A.; Jørgensen, J. K.; van der Wiel, M. H. D.; Garrod, R. T.; Müller, H. S. P.; Bjerkeli, P.; Bourke, T. L.; Calcutt, H.; Drozdovskaya, M. N.; et al. The ALMA-PILS Survey: First Detections of Ethylene Oxide, Acetone and Propanal toward the Low-Mass Protostar IRAS 16293-2422. *Astron. Astrophys.* **2017**, *597*, A53.
- (21) Herbst, E.; Giles, K.; Smith, D. Is Interstellar Acetone Produced by Ion-Molecule Chemistry? *Astrophys. J.* **1990**, *358*, 468.
- (22) Wakelam, V.; Loison, J. C.; Herbst, E.; Pavone, B.; Bergeat, A.; Béroff, K.; Chabot, M.; Faure, A.; Galli, D.; Geppert, W. D.; et al. The 2014 KIDA Network for Interstellar Chemistry. *Astrophys. J., Suppl. Ser.* **2015**, *217*, 20.
- (23) Goulay, F.; Derakhshan, A.; Maher, E.; Trevitt, A. J.; Savee, J. D.; Scheer, A. M.; Osborn, D. L.; Taatjes, C. A. Formation of Dimethylketene and Methacrolein by Reaction of the CH Radical with Acetone. *Phys. Chem. Chem. Phys.* **2013**, *15*, 4049-4058.
- (24) Shannon, R. J.; Taylor, S.; Goddard, A.; Blitz, M. A.; Heard, D. E. Observation of a Large Negative Temperature Dependence for Rate Coefficients of Reactions of OH with Oxygenated Volatile Organic Compounds Studied at 86-112 K. *Phys. Chem. Chem. Phys.* **2010**, *12*, 13511-13514.
- (25) Blázquez, S.; González, D.; García-Sáez, A.; Antiñolo, M.; Bergeat, A.; Caralp, F.; Mereau, R.; Canosa, A.; Ballesteros, B.; Albaladejo, J.; et al. Experimental and Theoretical Investigation on the OH + CH₃C(O)CH₃ Reaction at Interstellar Temperatures (T = 11.7–64.4 K). *ACS Earth Space Chem.* **2019**, *3*, 1873-1883.
- (26) Garrod, R. T.; Widicus Weaver, S. L.; Herbst, E. Complex Chemistry in Star-forming Regions: An Expanded Gas-Grain Warm-up Chemical Model. *Astrophys. J.* **2008**, *682*, 283-302.
- (27) Daugey, N.; Caubet, P.; Retail, B.; Costes, M.; Bergeat, A.; Dorthe, G. Kinetic Measurements on Methylidyne Radical Reactions with Several Hydrocarbons at Low Temperatures. *Phys. Chem. Chem. Phys.* **2005**, *7*, 2921-2927.
- (28) Daugey, N.; Caubet, P.; Bergeat, A.; Costes, M.; Hickson, K. M. Reaction Kinetics to Low Temperatures. Dicarbon + Acetylene, Methylacetylene, Allene and Propene from 77 ≤ T ≤ 296 K. *Phys. Chem. Chem. Phys.* **2008**, *10*, 729-737.
- (29) Hickson, K. M.; Loison, J.-C.; Bourgalais, J.; Capron, M.; Le Picard, S., D.; Goulay, F.; Wakelam, V. The C(³P) + NH₃ Reaction in Interstellar Chemistry. II. Low Temperature Rate

Constants and Modeling of NH, NH₂, and NH₃ Abundances in Dense Interstellar Clouds. *Astrophys. J.* **2015**, *812*, 107.

(30) Hickson, K. M.; Loison, J.-C.; Nuñez-Reyes, D.; Méreau, R. Quantum Tunneling Enhancement of the C + H₂O and C + D₂O Reactions at Low Temperature. *J. Phys. Chem. Lett.* **2016**, *7*, 3641-3646.

(31) Bourgalais, J.; Capron, M.; Kailasanathan, R. K. A.; Osborn, D., L.; Hickson, K., M.; Loison, J.-C.; Wakelam, V.; Goulay, F.; Le Picard, S., D. The C(³P) + NH₃ Reaction in Interstellar Chemistry. I. Investigation of the Product Formation Channels. *Astrophys. J.* **2015**, *812*, 106.

(32) Hickson, K. M.; Loison, J.-C.; Lique, F.; Kłos, J. An Experimental and Theoretical Investigation of the C(¹D) + N₂ → C(³P) + N₂ Quenching Reaction at Low Temperature. *J. Phys. Chem. A* **2016**, *120*, 2504-2513.

(33) Meng, Q. Y.; Hickson, K. M.; Shao, K. J.; Loison, J. C.; Zhang, D. H. Theoretical and Experimental Investigations of Rate Coefficients of O(¹D) + CH₄ at Low Temperature. *Phys. Chem. Chem. Phys.* **2016**, *18*, 29286-29292.

(34) Grondin, R.; Loison, J.-C.; Hickson, K. M. Low Temperature Rate Constants for the Reactions of O(¹D) with N₂, O₂, and Ar. *J. Phys. Chem. A* **2016**, *120*, 4838-4844.

(35) Nuñez-Reyes, D.; Hickson, K. M. A Low Temperature Investigation of the Gas-Phase N(²D) + NO Reaction. Towards a Viable Source of N(²D) Atoms for Kinetic Studies in Astrochemistry. *Phys. Chem. Chem. Phys.* **2018**, *20*, 17442-17447.

(36) Nuñez-Reyes, D.; Loison, J.-C.; Hickson, K. M.; Dobrijevic, M. A Low Temperature Investigation of the N(²D) + CH₄, C₂H₆ and C₃H₈ reactions. *Phys. Chem. Chem. Phys.* **2019**, *21*, 6574-6581.

(37) Ambrose, D.; Sprake, C. H. S.; Townsend, R. Thermodynamic Properties of Organic Oxygen Compounds XXXIII. The Vapour Pressure of Acetone. *J. Chem. Thermodyn.* **1974**, *6*, 693-700.

(38) Zhao, Y.; Truhlar, D. The M06 Suite of Density Functionals for Main Group Thermochemistry, Thermochemical Kinetics, Noncovalent Interactions, Excited States, and Transition Elements: Two New Functionals and Systematic Testing of Four M06-Class Functionals and 12 Other Functionals. *Theor. Chem. Acc.* **2008**, *120*, 215-241.

(39) Zhao, Y.; Truhlar, D. G. Density Functionals with Broad Applicability in Chemistry. *Acc. Chem. Res.* **2008**, *41*, 157-167.

(40) Guo, Y.; Riplinger, C.; Becker, U.; Liakos, D. G.; Minenkov, Y.; Cavallo, L.; Neese, F. Communication: An Improved Linear Scaling Perturbative Triples Correction for the Domain Based Local Pair-Natural Orbital Based Singles and Doubles Coupled Cluster Method [DLPNO-CCSD(T)]. *J. Chem. Phys.* **2018**, *148*, 011101.

(41) Kossmann, S.; Neese, F. Efficient Structure Optimization with Second-Order Many-Body Perturbation Theory: The RIJCOSX-MP2 Method. *J. Chem. Theory Comput.* **2010**, *6*, 2325-2338.

(42) Neese, F. The ORCA Program System. *WIREs Comput. Mol. Sci.* **2012**, *2*, 73-78.

(43) Neese, F. Software update: The ORCA program system—Version 5.0. *WIREs Comput. Mol. Sci.* **2022**, *12*, e1606.

(44) Hanwell, M. D.; Curtis, D. E.; Lonie, D. C.; Vandermeersch, T.; Zurek, E.; Hutchison, G. R. Avogadro: An Advanced Semantic Chemical Editor, Visualization, and Analysis Platform. *J. Cheminf.* **2012**, *4*, 17.

(45) Joo, H.; Shevlin, P. B.; McKee, M. L. Computational Study of Carbon Atom (³P and ¹D) Reaction with CH₂O. Theoretical Evaluation of ¹B₁ Methylene Production by C (¹D). *J. Am. Chem. Soc.* **2006**, *128*, 6220-6230.

- (46) Liakos, D. G.; Guo, Y.; Neese, F. Comprehensive Benchmark Results for the Domain Based Local Pair Natural Orbital Coupled Cluster Method (DLPNO-CCSD(T)) for Closed- and Open-Shell Systems. *J. Phys. Chem. A* **2020**, *124*, 90-100.
- (47) Husain, D.; Kirsch, L. J. Study of Electronically Excited Carbon Atoms, C(2^1D_2), by the Attenuation of Atomic Emission, ($3^1P^{\circ}_1 \rightarrow 2^1D_2$). Part 1.-Collisional Deactivation of C(2^1D_2) by the Noble Gases. *Trans. Faraday Soc.* **1971**, *67*, 2886-2895.
- (48) Husain, D.; Ioannou, A. X. Collisional Removal of Atomic Carbon, C[$2p2(^3P_j)$], by Aldehydes and Ketones, Investigated by Time-Resolved Atomic Resonance Absorption Spectroscopy in the Vacuum Ultra-Violet. *J. Photo. Photobio. A* **1999**, *129*, 1-7.
- (49) Bergeat, A.; Loison, J.-C. Reaction of Carbon Atoms, C($2p2, ^3P$) with C₂H₂, C₂H₄ and C₆H₆: Overall Rate Constant and Relative Atomic Hydrogen Production. *Phys. Chem. Chem. Phys.* **2001**, *3*, 2038-2042.
- (50) Le, T. N.; Lee, H.-y.; Mebel, A. M.; Kaiser, R. I. Ab Initio MO Study of the Triplet C₃H₄ Potential Energy Surface and the Reaction of C(3P_j) with Ethylene, C₂H₄. *J. Phys. Chem. A* **2001**, *105*, 1847-1856.
- (51) Langford, A. O.; Moore, C. B. Reaction and Relaxation of Vibrationally Excited Formyl Radicals. *J. Chem. Phys.* **1984**, *80*, 4204-4210.
- (52) Krasnoperov, L. N.; Chesnokov, E. N.; Stark, H.; Ravishankara, A. R. Unimolecular Dissociation of Formyl Radical, HCO \rightarrow H + CO, Studied over 1–100 Bar Pressure Range. *J. Phys. Chem. A* **2004**, *108*, 11526-11536.
- (53) Hersant, F.; Wakelam, V.; Dutrey, A.; Guilloteau, S.; Herbst, E. Cold CO in Circumstellar Disks. *Astron. Astrophys.* **2009**, *493*, L49-L52.
- (54) Semenov, D.; Hersant, F.; Wakelam, V.; Dutrey, A.; Chapillon, E.; Guilloteau, S.; Henning, T.; Launhardt, R.; Piétu, V.; Schreyer, K. Chemistry in Disks IV. Benchmarking Gas-Grain Chemical Models with Surface Reactions. *Astron. Astrophys.* **2010**, *522*, A42.
- (55) Ruaud, M.; Loison, J. C.; Hickson, K. M.; Gratier, P.; Hersant, F.; Wakelam, V. Modelling Complex Organic Molecules in Dense Regions: Eley-Rideal and Complex Induced Reaction. *Mon. Not. R. Astron. Soc.* **2015**, *447*, 4004-4017.
- (56) Ruaud, M.; Wakelam, V.; Hersant, F. Gas and Grain Chemical Composition in Cold Cores as Predicted by the Nautilus Three-Phase Model. *Mon. Not. R. Astron. Soc.* **2016**, *459*, 3756-3767.
- (57) Manigand, S.; Coutens, A.; Loison, J. C.; Wakelam, V.; Calcutt, H.; Müller, H. S. P.; Jørgensen, J. K.; Taquet, V.; Wampfler, S. F.; Bourke, T. L.; et al. The ALMA-PILS Survey: First Detection of the Unsaturated 3-Carbon Molecules Propenal (C₂H₃CHO) and Propylene (C₃H₆) Towards IRAS 16293–2422 B. *Astron. Astrophys.* **2021**, *645*, A53.
- (58) Coutens, A.; Loison, J. C.; Boulanger, A.; Caux, E.; Müller, H. S. P.; Wakelam, V.; Manigand, S.; Jørgensen, J. K. The ALMA-PILS survey: First Tentative Detection of 3-Hydroxypropenal (HOCHCHCHO) in the Interstellar Medium and Chemical Modeling of the C₃H₄O₂ Isomers. *Astron. Astrophys.* **2022**, *660*, L6.
- (59) Wakelam, V.; Dartois, E.; Chabot, M.; Spezzano, S.; Navarro-Almida, D.; Loison, J. C.; Fuente, A. Efficiency of Non-Thermal Desorptions in Cold-Core Conditions. *Astron. Astrophys.* **2021**, *652*, A63.
- (60) Hoyermann, K.; Sievert, R. The Reactions of Alkyl Radicals with Oxygen Atoms: Identification of Primary Products at Low Pressure. *Symp. (Int.) Combust.* **1979**, *17*, 517-524.
- (61) Shannon, R. J.; Caravan, R. L.; Blitz, M. A.; Heard, D. E. A Combined Experimental and Theoretical Study of Reactions between the Hydroxyl Radical and Oxygenated Hydrocarbons Relevant to Astrochemical Environments. *Phys. Chem. Chem. Phys.* **2014**, *16*, 3466-3478.

- (62) Woon, D. E.; Herbst, E. On the Stability of Interstellar Carbon Clusters: The Rate of the Reaction between C_3 and O. *Astrophys. J.* **1996**, *465*, 795-799.
- (63) Lin, Z.; Talbi, D.; Roueff, E.; Herbst, E.; Wehres, N.; Cole, C. A.; Yang, Z.; Snow, T. P.; Bierbaum, V. M. Can Interstellar Propene (CH_3CHCH_2) be Formed via Gas-Phase Reactions? *Astrophys. J.* **2013**, *765*, 80.
- (64) Savic, I.; Gerlich, D. Temperature Variable Ion Trap Studies of $C_3H_n^+$ with H_2 and HD. *Phys. Chem. Chem. Phys.* **2005**, *7*, 1026-1035.
- (65) Loison, J.-C.; Wakelam, V.; Gratier, P.; Hickson, K. M. Gas-grain Model of Carbon Fractionation in Dense Molecular Clouds. *Mon. Not. R. Astron. Soc.* **2020**, *498*, 4663-4679.
- (66) Markwick, A. J.; Millar, T. J.; Charnley, S. B. CH_2DCCH Along the TMC-1 Ridge. *Astron. Astrophys.* **2002**, *381*, 560-565.
- (67) Marcelino, N.; Cernicharo, J.; Agundez, M.; Roueff, E.; Gerin, M.; Martin-Pintado, J.; Mauersberger, R.; Thum, C. Discovery of Interstellar Propylene (CH_2CHCH_3): Missing Links in Interstellar Gas-Phase Chemistry. *Astrophys. J.* **2007**, *665*, L127-L130.
- (68) Hickson, K. M.; Wakelam, V.; Loison, J.-C. Methylacetylene (CH_3CCH) and Propene (C_3H_6) Formation in Cold Dense Clouds: A Case of Dust Grain Chemistry. *Mol. Astrophys.* **2016**, *3-4*, 1-9.
- (69) Sabbah, H.; Biennier, L.; Sims, I. R.; Georgievskii, Y.; Klippenstein, S. J.; Smith, I. W. M. Understanding Reactivity at Very Low Temperatures: the Reactions of Oxygen Atoms with Alkenes. *Science* **2007**, *317*, 102-105.
- (70) Savee, J. D.; Welz, O.; Taatjes, C. A.; Osborn, D. L. New Mechanistic Insights to the $O(^3P)$ + Propene Reaction from Multiplexed Photoionization Mass Spectrometry. *Phys. Chem. Chem. Phys.* **2012**, *14*, 10410-10423.

Supporting information file for

Kinetic Study of the Gas-Phase Reaction between Atomic Carbon and Acetone. Low Temperature Rate Constants and Hydrogen Atom Product Yields

Kevin M. Hickson,^{1,*} Jean-Christophe Loison,¹ and Valentine Wakelam²

¹Institut des Sciences Moléculaires ISM, CNRS UMR 5255, Univ. Bordeaux, 351 Cours de la Libération, F-33400, Talence, France

²Laboratoire d'astrophysique de Bordeaux, CNRS, Univ. Bordeaux, B18N, allée Geoffroy Saint-Hilaire, F-33615 Pessac, France

Geometries and frequencies of the stationary points involved in the C(³P) + CH₃COCH₃ reaction obtained at the M06-2X/aug-cc-pVTZ level of theory.

Geometries in Cartesian coordinates

Reactants and Products

CH₃COCH₃

C	0.00000001870384	-0.00000000422835	0.18602837740653
O	-0.00000014265663	-0.00000006240400	1.39089204428984
C	0.00000680803691	1.28242233539903	-0.61052890082265
C	-0.00000677256864	-1.28242231982573	-0.61052891149649
H	0.00027610415161	2.13692371889576	0.05904464284650
H	-0.00027597261171	-2.13692366518312	0.05904468196830
H	0.87688534661262	1.31561307911012	-1.25862162253853
H	-0.87717918885784	1.31586626815558	-1.25819385241016
H	-0.87688537049766	-1.31561309983610	-1.25862152655879
H	0.87717916968751	-1.31586625008319	-1.25819393268455

HCCHCOCH₃

C	-0.32284520495004	0.10985361037353	0.06496777966095
O	-0.93160590621430	0.12415554849061	1.10600843444849
C	0.24427371635435	1.35580942098570	-0.56221636913770
C	-0.10942151762672	-1.18537455080587	-0.65425071237227
H	0.01841252901913	2.21263336599183	0.06464848958516
H	1.32256476810597	1.24893561257046	-0.68282060039485
H	-0.17915919952443	1.49286535898829	-1.55750866011179
C	0.52773258330259	-1.27647968549415	-1.79076432049861
H	0.80630707232789	-2.04754443118176	-2.48959922580050
H	-0.53077134589444	-2.05715117231864	-0.15624792657888

CH₃CO

C	-0.96838708495203	-0.66177367442313	0.00000078566803
C	0.00018648349808	0.49407271025227	0.00000244228037
O	1.17299516746654	0.46561086558913	-0.00000299443596
H	-0.43472508407789	-1.61261293010581	0.00000070416548
H	-1.60481650590892	-0.57539675124910	0.87856322559353
H	-1.60481297602576	-0.57539522006337	-0.87856416327143

CCH₃

C	-2.59449501429966	1.68588554347691	0.04316231336064
H	-1.50145602031574	1.74766547754805	0.01793601398080
H	-2.97782061291938	2.73154817677500	0.03366698248128
H	-3.00024969750658	1.19188846828416	-0.84602630144415
C	-3.20091114115863	1.35784550591586	1.30477963892142

³CH₃CCH₃

C	0.00000006799431	-0.00000129000408	-0.03771929523381
C	0.00003334436765	1.34116324513297	-0.63234430402035
C	-0.00003338267224	-1.34116452506699	-0.63234723065241
H	0.00009170706693	2.11394420578366	0.13703158373309
H	-0.00009233909526	-2.11394717803340	0.13702695259266
H	0.88312222001366	1.50708416699662	-1.26212831539207
H	-0.88308344254480	1.50715813912857	-1.26206947543592
H	-0.88312207699113	-1.50708373878005	-1.26213193446062
H	0.88308358306088	-1.50715835185730	-1.26207244013057

¹CH₃CCH₃

C	-1.04789209463613	-0.49425235228936	-0.14870688218515
C	-0.08474595046238	0.60655380724189	-0.27151328873167
C	1.29735602587700	0.13247554650663	-0.12791913822487
H	1.44703474603788	-0.83706148045045	0.36574140533310
H	1.99770279966192	0.88469850479069	0.22824313613638
H	-0.67043551143556	-1.51281224672889	-0.31080688125870
H	-1.26633297154745	-0.40419947676005	0.93170700760220
H	-1.99573561247981	-0.32482955131073	-0.65475365714804
H	1.53616854998453	-0.01463301439973	-1.19763413482325

CH₃CCO

C	0.10042726297591	1.16860803964083	0.84959068127642
C	-0.08428685218921	0.65084016145083	1.97652561195830
C	0.29607935458759	1.67443902585970	-0.49495069410729
H	0.47647160426826	2.74781314472088	-0.52451028986164
H	1.13483838574479	1.16038571642066	-0.96952583834220
H	-0.58335795095514	1.44900852239294	-1.10306285507223
O	-0.25638780443220	0.18201638951415	3.04976738414865

CH₂CCOCH₃

C	0.01111967658826	0.09744950414822	0.12452014917168
---	------------------	------------------	------------------

C	-0.49412262597738	0.42187972341790	1.48809590167114
C	0.50919913204491	1.09836785489686	-0.59291745960956
C	-0.08861581341910	-1.33497714775790	-0.30611835674158
H	0.53383158982730	2.10094746101929	-0.18825349424557
H	0.45795802160876	-1.97563515052388	0.38608662047225
H	0.90013653942045	0.93750130084678	-1.58953104941001
H	-1.12824629778640	-1.66231109181640	-0.28994928941910
H	0.31259169479000	-1.46699417444436	-1.30888434984032
O	-0.94552141539680	-0.32349860808650	2.27952922135107

CH₃CCH₂

C	0.43774665947813	0.26846974848431	-1.13401338274001
C	0.08081970000464	1.10571284525637	-2.06845066440994
C	0.07588164831151	-1.07064981196536	-0.65364283375308
H	-0.28483724171526	-1.03043483098718	0.37443272839324
H	-0.71372356038730	-1.50413286968462	-1.27722707526802
H	0.93584126684096	-1.74029868744683	-0.67674177408881
H	0.54862709958288	2.07639157475675	-2.18344244853136
H	-0.70888557211557	0.85485203158656	-2.77747454960201

CH₃

C	-0.70372357606606	1.18654111678269	-0.00005833245105
H	-0.70392912723809	0.22215060857474	-0.47829875439109
H	-0.70309120365291	2.08307218215012	-0.59589698537590
H	-0.70309310774294	1.25481377899245	1.07425224461803

HCO

C	-0.75931040142755	0.46707027306888	3.74746918555020
O	-0.88701919150079	-0.60908520484423	3.31157666395112
H	-0.22645040707167	1.30018493177535	3.22146415049867

CO

C	0.00000000000000	0.00000000000000	-0.64095512334366
O	0.00000000000000	0.00000000000000	0.48043012334366

CH₃CHCH₂

C	-1.13117731438409	-0.50304606783484	-0.00000007737906
C	0.00003244622660	0.47546729381995	-0.00000015594099
C	1.28305132497653	0.14730972848395	0.00000001396368
H	1.59680126178830	-0.89001897187121	-0.00000008653904
H	2.05991253087391	0.89934665153453	0.00000009567141
H	-0.27130028328953	1.52676225069718	0.00000020396423
H	-0.76326937018507	-1.52796761844465	0.00000010986960
H	-1.76623667917448	-0.36388145568398	0.87652663560215
H	-1.76623691683216	-0.36388181070094	-0.87652673921198

H₂CCCH₂

C	-0.00000003598378	-0.00000008390851	-0.00000000493640
C	-0.00000007095097	-0.00000001289853	1.29929676163271
C	-0.00000000231002	-0.00000015946924	-1.29929676527984
H	0.00000007707970	0.92817085726923	1.85551889701515
H	0.00000001275505	-0.92817080901590	1.85551901121975
H	0.92817084738687	0.00000013617379	-1.85551892747881
H	-0.92817082797685	0.00000007184914	-1.85551897217256

CH₂CCO

C	0.80855434690393	-1.64706437466224	0.00000001417645
C	-0.00005348679437	-0.61074604739055	0.00000002184009
C	-0.27940664776765	0.64581521702713	0.00000000086302
O	-0.68659837560138	1.73417659841576	-0.00000001248457
H	1.88991096433432	-1.53763544000684	-0.00000000639553
H	0.42827719892514	-2.66369495338325	-0.00000001799946

Intermediates

MIN1

C	-0.16352211755793	0.20987034760863	-0.31347534523821
C	-0.22108731947873	0.60236165019641	2.60218793743764
C	0.16596622468619	1.35393460329517	-1.16985388303839
C	-0.30274581186853	-1.22610202007185	-0.57725177251872
H	0.18803097483591	2.27950318802880	-0.59332640275855
H	-0.56043093802296	-1.77050076720897	0.33243336540257
H	1.14916836883768	1.23753514595904	-1.64254044966168
H	-0.56802446948755	1.48513982200174	-1.97455538499410
H	-1.08803695346301	-1.42985576954546	-1.31559224520469
H	0.62774948762801	-1.65888888964936	-0.96544454600873
O	-0.39939008117693	-0.47271777547714	2.87468376924972

MIN2

C	-0.01194404223955	-0.02597801455009	0.19465330992908
O	-0.04188676553894	0.02640611905240	1.39706870818044
C	0.01671297907638	1.23202065357893	-0.64521316629181
C	0.00837181977552	-1.33474868937989	-0.55368702089927
H	-0.02343448856040	2.11624650675674	-0.01486720753788
H	-0.05868664960317	-2.16247028855417	0.14575591996550
H	0.94332789297146	1.25565346279867	-1.22998577516096
H	-0.83427123642990	1.23783977258277	-1.33326824392970
H	-0.81550479473865	-1.37170300786101	-1.26824927191851
H	0.92979217075018	-1.40813154102917	-1.13499235821083
C	0.26397582353708	0.64443628780483	-3.30903273692603

MIN3

C	-0.11065678283129	0.20084104570905	0.07204906715194
C	-0.19674788130291	0.49055199208174	1.47955559683294

C	0.13980670173191	1.29770743461363	-0.89420375911534
C	-0.27245911151351	-1.19427246281092	-0.42480906766823
H	0.26328253228358	2.25113644142102	-0.38679070826301
H	-0.48855232802888	-1.88493034655268	0.38594122745694
H	1.03405342746663	1.08835496395339	-1.48797438814062
H	-0.68907078041443	1.37726906024182	-1.60383156389423
H	-1.07766023163798	-1.24093266328813	-1.16295358105459
H	0.63813720678993	-1.51859557990479	-0.93702996547719
O	-0.39083527774303	-0.25219401236414	2.38925994087140

MIN4

C	0.12059702647454	-0.06664226190554	0.01713671986137
O	0.66907895736751	0.11194041280523	1.07178484200812
C	-0.32182936744251	1.11833137827412	-0.84711006255168
C	-0.12944035086533	-1.43602786417605	-0.55694765327389
H	-0.38186105839683	1.99949265258287	-0.20185223750340
H	0.36396468250534	-2.19236255336504	0.04587404087216
H	1.70002298869454	1.54878802777759	-1.92272815132838
H	-1.31335825964576	0.91963717733416	-1.26255910876161
H	-1.20469948784583	-1.62392633990840	-0.57629843515892
H	0.22474134906780	-1.47480213037206	-1.58775497806642
C	0.64923622908652	1.30514276215312	-1.93136281889733

MIN 5

C	-0.15657516278513	0.46738146260138	0.51822439119640
C	0.02617229290588	0.86784709033301	1.88501828989984
C	-0.02134511638168	1.16825987432879	-0.77903011957709
H	-0.12077152005574	2.24868230694659	-0.63360607947005
H	0.95445648352060	0.96322208578218	-1.21404985786900
H	-0.79122692607216	0.83548951140384	-1.47363032822508
O	-1.24691909481922	0.66812698493920	1.35851572059409
C	0.50404549748821	0.16607807352891	3.09888852152559
H	1.56049707264839	0.37409976425595	3.25610293104664
H	-0.05072595943572	0.49574275425308	3.97622027957707
H	0.37357398068656	-0.91476987087293	2.98448958550159

MIN6

C	-0.12463087188148	0.15893614946121	0.03938980393740
C	-0.19338575786233	0.52661731439984	1.42913457298081
C	0.11831461633300	1.17680714857325	-0.97427097100752
C	-0.29244153014339	-1.26507253472189	-0.36195727801087
H	-0.51421459749441	-1.88170777654750	0.50533793004828
H	-1.09280268111813	-1.35974457669740	-1.09966532522754
H	0.61853533017613	-1.62978596814996	-0.84457991940526
O	-0.38255954998991	-0.27202769712582	2.33646225833097
H	-0.70243955113243	1.66461271153213	-1.48246915070644
H	1.12288208681322	1.40040012270234	-1.30746214376535

H -0.05856836670029 1.59904673697382 1.64401615492550

MIN7

C -0.54364038222218 0.80548793677536 0.88061628083906
O -1.73634667571567 0.53793031881531 0.98399923502504
C 0.14441224373359 1.79620911500529 1.78268202877433
H 0.58828023508339 2.59626056207417 1.18947957651043
H 0.95296972189795 1.30479567212607 2.32469735092881
H -0.57332542931216 2.21084258635973 2.48482128166017
C 0.23942819919762 0.15971478089893 -0.12812321508159
C -0.09900576590784 -0.83444473347858 -1.14550506302486
H -0.22107215699801 -0.36586251375677 -2.12573067659317
H 0.68219614853484 -1.59012254026429 -1.23785803288996
H -1.04115795999155 -1.32205255665525 -0.88202106694829

MIN8

C -0.08245107525222 0.09718581310793 0.21262805746180
C 0.15556939368973 0.22893019611552 1.64072941120433
C -0.02847987738273 1.29708002069527 -0.68095854588172
C -0.02580943144878 -1.24573312012321 -0.44629829017121
H -0.17910371561867 2.20677756050973 -0.10681936762173
H -0.17464417576616 -2.03490998807569 0.28504241871462
H 0.94640811668560 1.34104493827751 -1.16816505974155
H -0.79006585082403 1.22225470553272 -1.45890777893067
H -0.78771865733780 -1.31628101630602 -1.22436600785401
H 0.94907402111123 -1.37639133983094 -0.91765369845970
O -1.13348127305616 0.19497810319719 1.29398165997984

MIN9

C -0.13494793441388 0.11643782715097 0.23828590867773
C 0.34268871008592 -0.50101345339544 2.46730298713615
C -0.09727839069314 1.32227079371883 -0.61382128980674
C -0.01913466719471 -1.28521054802228 -0.20894926366721
H -0.55173804526651 2.16774340314182 -0.09885798866409
H -0.68859959844050 -1.93777523378295 0.35468497107859
H 0.93092336089497 1.60519727297025 -0.87059572144875
H -0.63290485077226 1.14391278966461 -1.54439958777963
H -0.25341800048811 -1.35102672168265 -1.26872542576091
H 0.99399121199514 -1.66981611735746 -0.04312424714455
O 0.11041920429307 0.38927898759431 1.58819965737942

MIN10

C 0.01083177769884 -0.09398772883272 0.19921141952008
O -0.24055923127547 0.03752761779081 1.38858212693245
C 0.23959083055543 1.07406444022281 -0.62992149532193
C 0.10114249561133 -1.45450492316359 -0.44983506153444
H 0.16276866883957 2.02467025359794 -0.11021158093282

H	-0.09941950411689	-2.22148509661805	0.29214198140943
H	1.58571895264801	1.02723715215505	-2.38209893856354
H	-0.61500655780464	-1.53072773320592	-1.26932371853483
H	1.09365270646054	-1.60254442255108	-0.87834809934347
C	0.55818047052610	1.02951799791307	-2.04306509507652
H	-0.21398060914283	1.12738244269167	-2.79453153855441

Transition states

TS1

C	-0.02157759685125	0.15416441172135	-0.18624044746157
C	-0.27484824473130	0.61209851551254	2.01809300507047
C	0.18011166386765	1.34540123564966	-1.01585112532492
C	-0.25297033948131	-1.25866325901748	-0.50422352372878
H	0.29884354172314	2.23140773542231	-0.39185686405879
H	-0.37235091646954	-1.84948369421169	0.40529545680152
H	1.07366040313958	1.25619933532410	-1.64471010055112
H	-0.67060643749137	1.51996466559346	-1.68558790191707
H	-1.15859981754281	-1.39242811675229	-1.10771394811489
H	0.58245844526398	-1.68722891124239	-1.07006853752488
O	-0.53482322662675	-0.31649604489956	2.61207678551005

TS2

C	0.27262608519621	-0.28210094987248	0.11355480680924
O	0.66255141723526	-0.05409084897067	1.22940256438585
C	0.04801399893804	0.83107549636850	-0.88585851350720
C	-0.00437921828531	-1.69364011086630	-0.34686076467446
H	-0.67024484287591	1.53568744949690	-0.46816767144953
H	0.15843076335015	-2.40176787408041	0.46080382064166
H	0.98646602239344	1.36627518160999	-1.02643923215456
H	-0.31193973849281	0.46747929000778	-1.84626933586882
H	-1.03875434038494	-1.76895603072388	-0.69841585590709
H	0.66518091895966	-1.93489091387362	-1.18010756510521
C	-0.76796372403378	-1.95102254649570	-2.99087661786977

TS3

C	-0.01216756818671	-0.00057101884850	0.10486339588755
C	-0.02402684122938	0.63179224530685	1.38792015913411
C	0.24084250956662	1.18843535068251	-0.74323424121513
C	-0.19212741755148	-1.42048661447564	-0.26008155656999
H	-0.40378559744557	-2.02923476636087	0.61660830765342
H	-1.00739471244639	-1.52925401859614	-0.97956987477955
H	0.70831048619003	-1.80225494082355	-0.74929176708862
O	-0.16624115489786	0.32436142764931	2.53226410645961
H	-0.57818901674412	1.55763652267879	-1.35712041947901
H	1.22037124145208	1.28645811550847	-1.20643730809714
H	0.21440807129278	1.79311769727878	0.65407919809475

TS4

C	0.16563369185183	0.04209239904451	0.39075589142075
C	0.40146613254568	0.19671602770864	1.78873918182217
C	0.15236792559749	1.23958925902647	-0.49711257592622
C	-0.04376476899877	-1.30121532115649	-0.22213071055923
H	-0.58716483653565	1.94392771848778	-0.11431222139455
H	-0.07432246240199	-2.07877010922965	0.53419463057264
H	1.12408791990313	1.73318730321860	-0.44279013534460
H	-0.08242506607034	0.99225164074656	-1.53087395182665
H	-0.95981775327640	-1.31496964683094	-0.81693322154914
H	0.78911877323246	-1.49262263804576	-0.90483209417500
O	-0.88517955584746	0.03981336703027	1.81529520695983

TS5

C	-0.57723961983756	0.25597434047492	0.02162043946092
C	-0.30363336686632	-0.46158003066576	1.51885275244909
C	0.15414940613164	1.42474628000417	-0.51896294624965
H	0.68186798595266	1.93939628019393	0.28798793726087
H	0.86940896835157	1.10927908747411	-1.27590097916773
H	-0.55559324388937	2.11721941019613	-0.97257875347054
O	-1.41618149315962	0.30861986652782	1.03572035052099
C	0.18330645844411	-1.44139373544678	0.11187264900726
H	0.96855374157916	-1.93131786725359	0.69106491708572
H	-0.65010296637757	-2.12144304575898	-0.04412863225107
H	0.64546412967131	-1.19950058574596	-0.85554773464586

TS6

C	0.37930005978385	-0.67321093906050	-0.13192750876799
C	-0.20490492922462	0.49587562961606	0.34527784676188
C	-0.01748791108349	-1.70025597309374	-1.10766404084329
H	-0.96284783873277	-1.42940602418063	-1.58606032868157
H	0.76258459957178	-1.79481474051078	-1.86385312726609
H	-0.12655635364395	-2.66720684538076	-0.61599316984841
O	-1.06805895446058	-0.37866835182483	0.84942826433979
C	0.22834466271520	1.78660172600969	0.91427004913341
H	0.75360731685972	2.37892309997907	0.16842479853088
H	-0.64247727309253	2.34378722857347	1.25767255778346
H	0.89849662130739	1.63837518987294	1.77042465885793

TS7

C	-0.16920368622223	0.65023005175528	1.15617291562314
C	-0.26573174974063	-1.61687498669426	-0.18426036627984
O	0.64855022859571	0.55866893344910	2.05312399896373
C	0.15784527859469	1.46231961037544	-0.42307796776448
H	-0.73173940753021	2.00409662095873	-0.72260664930097
H	0.63005624635221	0.96754202861226	-1.27444105909187

H	0.89633511470446	2.12893894827580	0.02434417254563
H	-0.08863773751584	-1.70774221549377	-1.25556717830842
H	-1.09808054754365	-2.27146610052982	0.07904369283376
H	0.61948609793627	-1.95024355163457	0.36209102395589
C	-0.59887983763077	-0.22546933907419	0.18517741682344

TS8

C	-1.15757098986948	0.01618966361030	1.33013514538973
O	-1.79173802275774	0.23982010983573	2.29813445048962
C	0.10268602577897	1.87232504537468	1.08365203271864
H	-0.56158596494367	2.40340854120599	0.41685652163180
H	1.06937080114373	1.59049354639355	0.69360648843823
H	0.03700653882049	2.10874957816886	2.13417465748673
C	-0.77999929776105	-0.70238013862638	0.28897412689358
C	0.16997316166137	-0.58551996068424	-0.81750229626533
H	1.19318555264065	-0.66810680078548	-0.43726331467693
H	0.02300468240991	-1.36674432525546	-1.55956776169207
H	0.08840569117681	0.39052336866239	-1.30414235121409

TS9

C	0.02448350751026	0.42574800620320	0.56970565997971
C	-0.13543811668171	0.47004080282159	1.85288889208921
C	0.23268436427164	1.31894917782047	-0.57416841807246
C	-0.13881174254197	-1.64140041235171	-0.47447500647789
H	0.61845482847078	2.29794690709183	-0.29628518431813
H	-0.43987821965822	-2.27302090354659	0.34667793634788
H	0.88660890823638	0.84933238811940	-1.30843829125514
H	-0.73225386346809	1.45852267506146	-1.07247665673276
H	-0.88868257386416	-1.40401522595671	-1.21563755696398
H	0.88060364023965	-1.73605214178374	-0.81967771390382
O	-0.30777073251457	0.23394872652080	2.99188633930739

TS10

C	-0.29987839300943	-0.17887124491863	0.48194239270653
O	-0.30880537180875	-1.13442607288596	-0.11295043913999
H	0.60868376481817	1.31329731780460	-0.36899195356653

TS11

C	-0.08890570239885	0.04563111784284	0.28587182751047
C	0.81648136000391	-0.00270414482523	2.14389665853944
C	0.06063000820920	1.28003824785828	-0.50427865090724
C	-0.15832929712199	-1.33042581774495	-0.25618233911434
H	-0.87202004222350	1.85333969849011	-0.50100467201856
H	-0.30821653028241	-2.04903708251015	0.54488693590739
H	0.83030390772269	1.91021675461725	-0.05014069504099
H	0.33607591103565	1.05743484826600	-1.53247521467542
H	-0.98533209523965	-1.41812360116061	-0.96953224597858

H	0.75612735140519	-1.58840697042606	-0.79600101562097
O	-0.38681487111025	0.24203694959255	1.63495941139881

TS12

C	-0.28273125451093	0.08581218035497	0.11529694825741
C	-0.00725209477758	-0.48336037466888	2.55186465119477
C	-0.02763589187501	1.33018568403370	-0.62015866744981
C	0.01167194329562	-1.29876707839591	-0.26040974856800
H	-0.39683410272052	2.18732664134082	-0.05819856567741
H	-0.08741761614116	-1.94653699580795	0.61495633377662
H	1.04472222228447	1.47680911158530	-0.79802155129218
H	-0.52373659012351	1.31201792942258	-1.59204604659397
H	-0.67519922586983	-1.65307985501928	-1.03092483386637
H	1.03177316551626	-1.39930629499819	-0.64849847645202
O	-0.08736055507780	0.38889905215282	1.72613995667097

TS13

C	-0.27974749649867	0.08527152187477	0.11097796096649
C	-0.06472185822333	-0.48253751629921	2.55071863787987
C	-0.01488039228403	1.32995064553898	-0.62041352007761
C	0.02768505576230	-1.29808490236967	-0.25978058717574
H	-0.30945035069812	2.19159893054588	-0.02220893211646
H	0.00195177965410	-1.93142298759167	0.63206922760636
H	1.04923265812210	1.43084334332358	-0.86589751460223
H	-0.57182698554192	1.35400352021768	-1.55932542444652
H	-0.69688648260559	-1.68936483257813	-0.97674889140901
H	1.02185713372948	-1.37725069984080	-0.71288856948575
O	-0.16321206141632	0.38699197717862	1.72349761286063

TS14

C	0.21789079861456	0.17145943073301	-1.30331086537127
C	0.08545693314143	1.17607051169649	-2.11247277934457
C	0.28772134641381	-0.88630279945121	-0.53004471874948
H	-0.25162204877023	-0.91977418917644	0.40729996701364
H	-1.04529363914429	-2.14075338486883	-1.21791495879958
H	1.02754363206515	-1.65415262254911	-0.71392538143456
H	0.68908458603392	2.06885505265471	-2.00826631673073
H	-0.63931160835436	1.14450800096138	-2.91792494658342

Frequencies in cm⁻¹

Reactants and products

CH ₃ COCH ₃	HCCHCOCH ₃	CH ₃ CO	CCH ₃	³ CH ₃ CCH ₃	¹ CH ₃ CCH ₃	CH ₃ CCO	CH ₂ CCOCH ₃	CH ₃ CCH ₂	CH ₃	HCO	CO	CH ₃ CHCH ₂	H ₂ CCCH ₂	CH ₂ CCO
94	114	110	509	157	245	34	151	178	432	1106	2271	193	370	120
166	164	469	896	159	268	168	188	321	1412	1994		430	370	256
386	273	870	1114	298	445	503	241	513	1413	2724		590	867	508
496	495	961	1314	855	677	530	404	905	3144			938	871	696
540	499	1049	1324	938	703	789	457	920	3321			947	871	960
808	541	1355	1448	950	952	848	596	942	3323			959	1014	1051
893	723	1459	2913	1056	1009	1064	754	1055				1036	1014	1073
901	745	1461	3020	1126	1155	1391	803	1109				1080	1122	1487
1089	858	1993	3065	1315	1208	1467	965	1389				1193	1420	1824
1127	911	3075		1395	1325	1473	1008	1424				1332	1484	2293
1251	1022	3171		1402	1342	1552	1031	1461				1406	2082	3111
1391	1053	3173		1460	1396	2214	1071	1476				1455	3152	3188
1399	1224			1463	1401	3059	1268	1764				1482	3156	
1464	1262			1471	1493	3105	1407	3037				1495	3233	
1471	1394			1474	1500	3139	1439	3095				1739	3233	
1475	1466			2982	2972		1477	3115				3066		
1495	1475			2988	2977		1491	3138				3120		
1846	1680			3026	3032		1717	3202				3150		
3060	1823			3028	3037		1951					3170		
3063	3067			3102	3149		3081					3179		
3121	3116			3104	3150		3144					3258		
3127	3132						3169							
3176	3181						3186							
3177	3272						3278							

Intermediates

MIN1	MIN2	MIN3	MIN4	MIN5	MIN6	MIN7	MIN8	MIN9	MIN10
53	87	92	67	144	129	79	168	128	126
74	114	139	91	162	198	137	216	136	167
86	152	247	236	233	268	186	362	200	255
93	201	259	329	251	304	194	375	260	382
136	240	355	392	426	357	400	426	309	425
165	390	419	523	449	411	574	449	368	513
175	499	589	592	788	498	586	629	553	552
317	543	789	788	799	615	769	793	699	577
855	806	944	800	972	831	957	949	927	706
945	885	961	922	1032	900	982	993	957	817
958	900	1010	1027	1081	963	1041	1014	984	949
1060	1081	1046	1068	1091	1002	1062	1094	1043	997
1131	1127	1290	1105	1169	1043	1140	1232	1169	1039
1318	1245	1312	1175	1189	1284	1368	1259	1329	1120
1398	1372	1396	1249	1392	1299	1383	1407	1367	1272
1406	1395	1409	1270	1398	1386	1422	1411	1418	1353
1461	1466	1466	1387	1474	1427	1453	1432	1420	1401
1466	1471	1469	1447	1476	1449	1464	1472	1458	1447
1474	1484	1486	1465	1478	1478	1471	1475	1473	1466
1478	1495	1498	1475	1479	1480	1480	1495	1486	1478
2242	1853	1844	1852	1583	1635	1645	1509	1491	1675
3004	3037	3047	3054	3047	3000	3046	3055	3021	3077
3009	3075	3051	3075	3048	3055	3081	3059	3040	3137
3047	3083	3092	3104	3132	3103	3107	3120	3102	3152
3050	3135	3099	3140	3134	3154	3129	3125	3116	3156
3120	3180	3169	3193	3168	3178	3144	3168	3163	3195
3125	3193	3177	3233	3168	3249	3190	3169	3171	3243

Transition states

TS1	TS2	TS3	TS4	TS5	TS6	TS7	TS8	TS9	TS10	TS11	TS12	TS13	TS14
-246	-75	-2061	-1046	-596	-2162	-864	-663	-529	-609	-1992	-681	-675	-672
16	74	107	166	174	99	37	89	66	355	29	90	95	258
105	85	188	222	226	159	197	169	121	2214	147	112	139	361
121	148	236	331	266	221	204	197	132		164	134	178	409
129	253	246	368	329	261	217	220	191		230	248	253	446
147	390	447	415	404	401	388	294	228		346	285	287	892
239	499	530	469	528	427	522	397	402		442	309	318	896
314	532	669	794	646	782	583	430	460		767	529	531	931
844	799	797	947	788	947	871	477	480		921	848	852	1000
947	886	866	993	937	980	876	581	540		949	953	958	1023
948	932	908	1033	985	1011	908	794	746		989	958	961	1101
1045	1074	971	1057	997	1058	1016	861	824		1023	1053	1051	1417
1126	1118	1037	1234	1043	1106	1064	930	986		1032	1126	1127	1475
1319	1240	1118	1256	1120	1299	1276	1051	1051		1305	1333	1335	2034
1395	1366	1281	1386	1333	1379	1360	1378	1389		1319	1398	1404	3138
1400	1387	1324	1406	1391	1395	1393	1423	1413		1405	1419	1423	3153
1459	1473	1398	1439	1424	1450	1439	1426	1430		1415	1459	1461	3217
1463	1478	1425	1470	1458	1466	1462	1429	1443		1463	1466	1467	3235
1471	1482	1470	1480	1474	1468	1465	1467	1467		1465	1473	1474	
1475	1487	1482	1489	1477	1484	1475	1487	1498		1483	1476	1478	
2147	1853	1756	1499	1531	1552	1716	1970	2097		1488	1545	1544	
3009	3032	1840	3061	2994	3016	3042	3042	3045		3027	3015	3018	
3014	3084	3054	3068	3061	3049	3052	3095	3113		3032	3017	3020	
3053	3086	3101	3116	3067	3125	3109	3122	3117		3081	3083	3087	
3056	3159	3104	3140	3133	3129	3130	3158	3153		3087	3097	3096	
3118	3171	3162	3161	3163	3143	3143	3283	3274		3163	3112	3109	
3127	3183	3183	3196	3175	3170	3210	3295	3287		3173	3143	3144	

